Accepted Manuscript

Crustal structure of the high Andes in the north Pampean flat slab segment from magnetic and gravity data

Marcos A. Sánchez, Diego Winocur, Orlando Álvarez, Andrés Folguera, Myriam P. Martinez

PII: S0895-9811(16)30323-6

DOI: 10.1016/j.jsames.2016.12.007

Reference: SAMES 1636

To appear in: *Journal of South American Earth Sciences*

Received Date: 12 December 2015

Revised Date: 16 July 2016

Accepted Date: 9 December 2016

Please cite this article as: Sánchez, M.A., Winocur, D., Álvarez, O., Folguera, A., Martinez, M.P., Crustal structure of the high Andes in the north Pampean flat slab segment from magnetic and gravity data, *Journal of South American Earth Sciences* (2017), doi: 10.1016/j.jsames.2016.12.007.

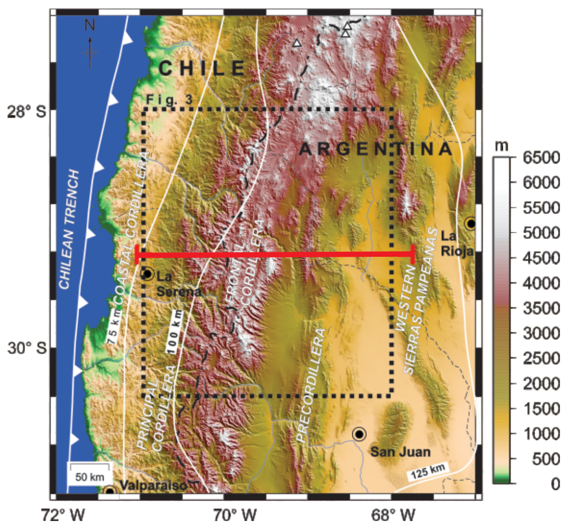

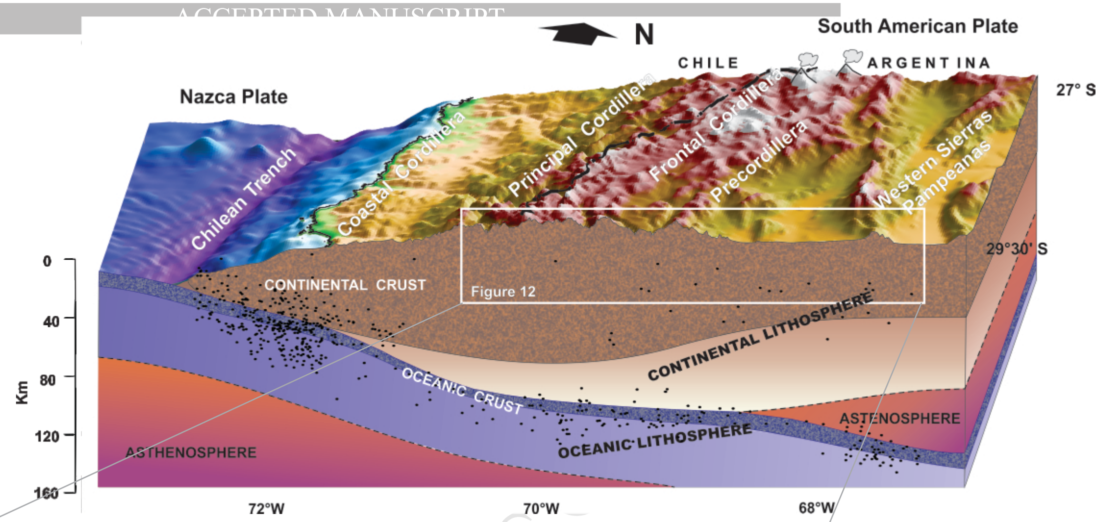

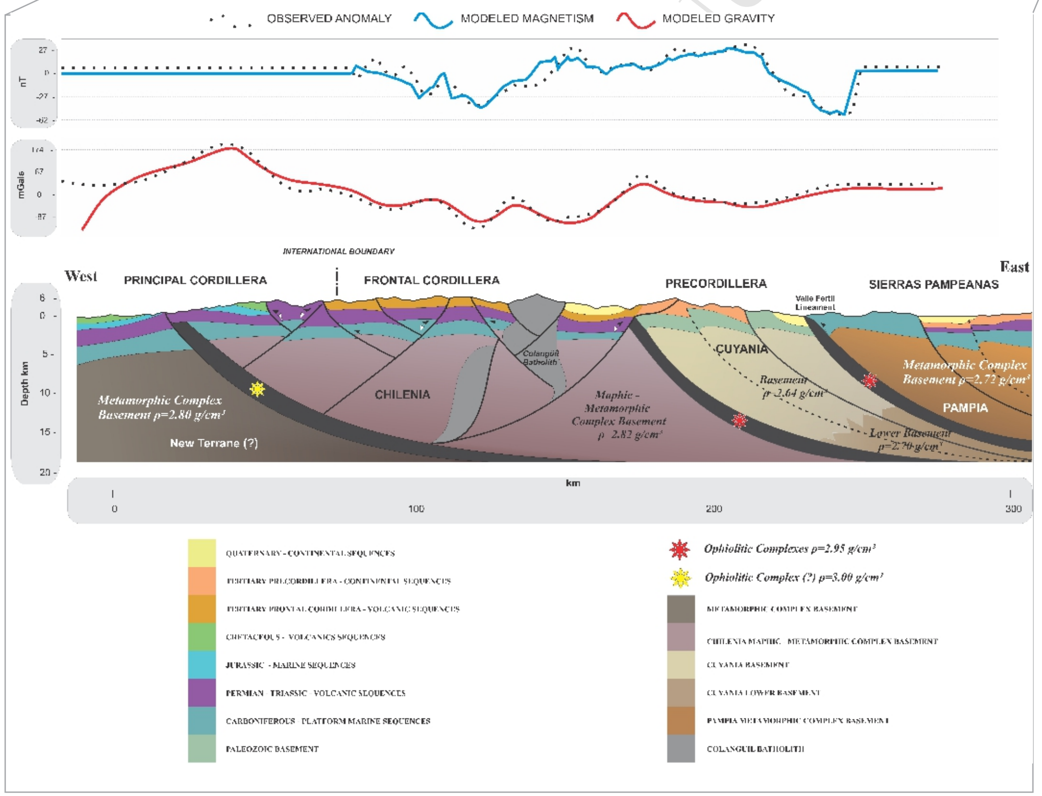

Graphical Abstract:

CRUSTAL STRUCTURE OF THE HIGH ANDES IN THE NORTH PAMPEAN FLAT SLAB SEGMENT FROM MAGNETIC AND GRAVITY DATA

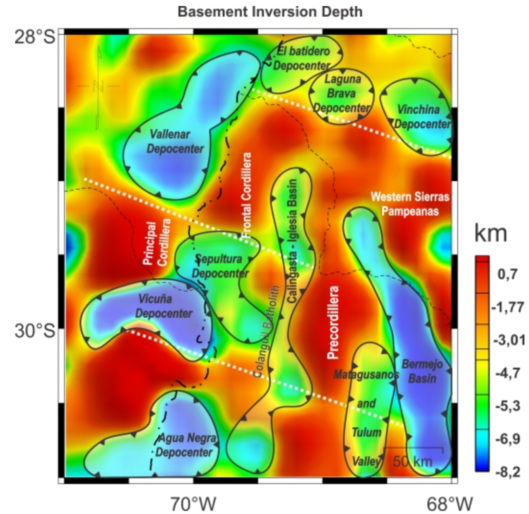

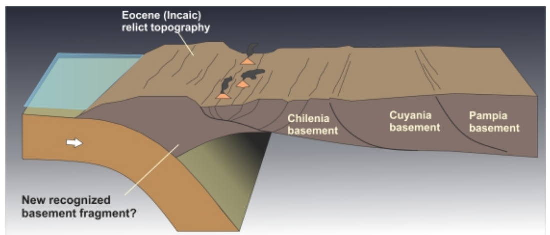

CRUSTAL STRUCTURE OF THE HIGH ANDES IN THE NORTH PAMPEAN FLAT SLAB SEGMENT FROM MAGNETIC AND GRAVITY DATA

Marcos A. Sánchez[1]*, Diego Winocur[2], Orlando Álvarez[1], Andrés Folguera[2], Myriam P. Martinez[1]

[1] CONICET. Instituto Geofísico y Sismológico Ing. Volponi, Universidad Nacional de San Juan, Ruta 12, km. 17, CP 5407, San Juan, Argentina.

[2] Inst. Estudios Andinos "Don Pablo Groeber". Dep. Cs. Geol. FCEN. U.B.A. Buenos Aires - Argentina.

* Corresponding author (e-mail: 1marcossanchez@gmail.com)

Keywords: Gravity, Magnetism, Basin geometry, Doña Ana Basin, late Oligocene, Miocene.

Abstract

The Main Andes at the northern Chilean-Pampean flat slab segment were formed by the inversion of late Oligocene to early Miocene extensional depocenters in Neogene times. Their structure, size and depth are loosely constrained by field data since these sequences have amalgamated forming an almost continuous blanket with scarce basement outcrops and their base is limitedly exposed. Satellite and aerial gravity and magnetic data are used in this work to define a 3D model that shows the basement structure at depth and adjust 2D structural sections previously based on field data. The results indicate complex basin geometry with depocenters of variable size and depth buried beneath Mesozoic (?)-Paleogene and Neogene sections. Additionally, previously proposed crustal heterogeneities across this orogenic segment are geophysically constrained with a new crustal heterogeneity identified on the basis of a modeled 2D crustal section. We propose hypothetically, that this crustal discontinuity could have played a role in controlling Paleogene extension at the hanging wall of an asymmetric rift basin, explaining the locus and development of the Doña Ana Basin. Finally, this work provides new information about Cenozoic structure and Paleozoic basement architecture, presumably derived from amalgamation history of one of the highest and more inaccessible regions of the Andes.

Keywords. Central Andes; aerial magnetic data; satellite gravity data; terrestrial gravity data; Paleogene basin architecture; Paleozoic basement structure

Introduction

The High Andes located across the Chilean-Pampean flat subduction zone are poorly explored due to their height with local peaks reaching the 7000 m (Figure 1). A complex structure produced by a thick-skinned array of structures partly derived from inversion of Late Triassic to Eocene-late Oligocene depocenters and new basement faults have produced an intricate mountain morphology with relay faults and abrupt changes in polarity (Mpodozis and Ramos 1989; see Charrier et al., 2007, for a synthesis). These High Andes through the Chilean-Pampean flat subduction zone can be separated in two morphostructural systems: the Principal Cordillera (Main Andes) to the west that comprises the drainage divide zone and is characterized by contractionally deformed Mesozoic rocks associated with variable decollement depths, one developed shallowly in Late Jurassic gypsum sequences and another located more deeply in an inverted Late Triassic extensional detachment, and the Frontal Cordillera to the east formed by Late Paleozoic to Paleogene extensive volcanoclastic sections exhumed in a thick skinned system (see Ramos et al., 2002 for a synthesis; and Martínez et al., 2015, for a newer approach). The Precordillera to the east is formed by Paleozoic imbricate series associated with variable decollement depths, detached in Cambrian and Silurian sequences in its northern section and related to the inversion of a Late Triassic extensional detachment in the south. This system has barely Paleogene cover and is considered to be part of a series of broken foreland mountain systems, including the Sierras Pampeanas in the easternmost foreland zone, that were uplifted at the time when the flat subduction segment started to develop since the last 17 Ma (Ramos et al., 1986, 2002).

The analysis of the structure in the High Andes has been considerably delayed in comparison with other neighbor segments due to their height and scarped morphology, reason by which geophysical potential methods and mainly those derived from aerial and satellite data in the last years, where no terrestrial measurements are available or scarce, proved to be useful. Particularly, we use in this work satellite and terrestrial gravity and aerial magnetic data, in combination with available geological data, to analyze the basement structure of the High Andes in the poorly explored northern part of the Chilean-Pampean flat subduction zone, producing 3D and 2D models. Thus, we present a broad 3D inversion model of the basement from the High Andes to the foreland zone in order to investigate the structure of the Paleogene depocenters. Additionally, we performed a 2D double inversion model, across a particular transect at 29°30'S in order to validate previous structural cross sections that were previously-only based on field data. This study is also aimed to show the applicability of combined satellite, aerial and terrestrial gravity and magnetic data to analyze upper to lower crustal structure in inaccessible mountain sectors.

Figure 1: *Study area in the northern Chilean-Pampean flat subduction zone represented over a DEM (90 x 90 m). White lines represent the contour lines of the Nazca Plate at depth (Mulcahy et al., 2014). The black dotted rectangle indicates the location of the study area. The profile modeled is indicated in red across the study area.*

Geological Setting

The Chilean-Pampean flat subduction zone is associated with a broad broken foreland system integrated by several morphostructural systems that comprise from the trench the Coastal Cordillera, the Main Cordillera in the drainage divide zone between Chile and Argentina, and the Frontal Cordillera, Precordillera and Pampean Ranges to the east on the Argentinean slope. Through this sector, Paleogene depocenters are exhumed in the Main Cordillera over Mesozoic marine and continental sections corresponding to the north-extension of the Neuquén Basin mainly developed on the Argentinean slope of the Andes (Vicente, 2005). To the east, the Frontal Cordillera exposes the basement of the Mesozoic sequences in a thick section of volcanic, volcanoclastic and intrusive rocks of Carboniferous to Permian-Triassic ages that comprise a suite of intrusives of the Elqui-Limarí and Colangüil batholiths and the Choiyoi Group (Figure 3) (Bissig et al., 2001; Charchaflié et al., 2007; Llambías y Sato, 1990). These rocks are covered unconformably by Oligo-Miocene volcanic and sedimentary sequences of the extensional Doña Ana Basin (Figure 4) (see Winocur et al., 2015, for a recent synthesis). Bissig et al. (2001) dated the volcanic rocks of the Doña Ana Formation by Ar/Ar methods obtaining ages comprehended between 27 and 17 Ma. Latter, Charchaflié et al., (2007) and Litvak (2009) reported K-Ar and Ar-Ar ages on these sections over the eastern Andean slope, confirming pre-existing ages and showing a wider extension of the basin on both slopes of the Andes. More recently, Winocur and Ramos (2008; 2011) and Winocur et al., (2014) proposed based on field criteria an extensional intra-arc control for these sections.

The Oligocene Doña Ana Formation defined initially by Thiele (1964) was lately subdivided by Maksaev et al., (1984) and Martin et al., (1995) into two units in the High Cordillera of Chile on the basis of K-Ar ages and an angular unconformity between them identified in field work. Thus, the Tilito Formation (27 to 22,1 Ma) composed of rhyolitic ignimbrite tuffs and dacitic lavas is separated from the Escabroso Formation (21 to 17 Ma), composed of andesitic to basaltic lavas, volcanic agglomerates and breccias, as part of the Doña Ana Formation. At the Argentinean side of the Andes, Ramos et al., (1987), Nullo (1988) and Marín y Nullo (1989) recognized these two units locally in the Cerro de las Tortolas and La Ortiga (Figure 4).

To the east of these Cenozoic depocenters, the Precordillera imbricates in an east-vergent system the basement of these sequences corresponding to marine and continental sedimentary rocks of Paleozoic ages (Baldis et al., 1982). Finally the Pampean ranges in the foreland zone are characterized by a deeper decollement that exposes Early to Late Paleozoic magmatic and metamorphic rocks. These eastern morphostructural systems were not affected by Oligocene extension, leaving the area of Cenozoic extension circumscribed to the High Andes region at these latitudes.

Figure 2: *3D block diagram with a DEM on top of it showing hypocenter location on a section at 29 ° 30 'S that signals the subhorizontal subduction of the Nazca Plate below the South American plate at the northern Chilean-Pampean flat slab segment. Black dots correspond to the relocation of seismic events obtained from International Seismological Centre (EHB Bulletin, http://www.isc.ac.uk). Morphostructural systems mentioned in the text are shown as a reference.*

Figure 3: *Geological map of the drainage divide area and eastern slope of the Andes from the Main Andes to the Frontal Cordillera and the northern Precordillera compiled from*

data from Furque (1998), Cardó et al., (1998, 2001), Caminos and Fauqué (2001), Fauqué et al., (2002) and Fauqué (2010). The red rectangle indicates the area covered by the figure 4 corresponding to the Valley del Cura region where one of the most detailed descriptions on the Cenozoic stratigraphy of the Frontal Cordillera is made. The location of profile displayed in Figure 12 is shown as a reference.

Figure 4: *Geological map of the Valle del Cura area in the Frontal Cordillera, showing the structure that affects and controls the Paleogene sequences and their basement constituting a doubly vergent system derived from Cenozoic inverted extensional systems (taken from Winocur et al., 2015). These field data were taken to construct the structural profile displayed in Figure 12.*

Data and methods

Gravity data

This study is based on a database which comprises 23680 gravity stations (Geophysical Seismological Institute of the National University of San Juan, IGSV). The database covers the central region of Argentina in an area between 27.5° to 36.5° S and from 71° to 65° W, extending outside of the boundaries of the study area which avoids border effects (Figure 5).

Figure 5: *Location of gravity and magnetic databases available in the region of study. Shaded rectangle indicates the area under study. Red dots indicate gravity data and yellow stars indicate the susceptibility data used in this work (Geophysical Seismological Institute of the National University of San Juan, IGSV). Grey lines correspond to the Nazca plate contours obtained by Mulcahy et al., (2014) shown as a reference.*

Each Gravity data station was measured using geodetic gravimeters with precisions of ± 0.1 mGal. With the purpose of ensure the accuracy of the measurements and to homogenize all stations obtained on different campaigns, each gravity station has been linked to the national altimetry network. This process allow avoiding any possible artifact due to problems in the leveling of the different sources, because all of these were referred to IGSN 71 network (International Gravity Standardization Net 1971) and are linked to the fundamental station Miguelete (Buenos Aires), through the nodal 145 City of San Juan and PF9 into the N24 line (Morelli et al., 1974) (more details about the homogenization and reductions to altimetry network are shown in Villella and Pacino 2010). This methodology allows making a proper data reduction for anomaly calculation using the classical corrections detailed below (Blakely, 1995; Hinze et al., 2005).

The theoretical or normal gravity, accounting for the mass, shape, and rotation of the earth is the predicted gravitational acceleration on the best-fitting terrestrial ellipsoidal surface. In this work we have used the 1980 Geodetic Reference System (GRS80) (Moritz, 1980), being the latest ellipsoid recommended by the International Union of Geodesy and Geophysics

The Somigliana closed-form formula (Somigliana, 1930) for the theoretical gravity g_T on this ellipsoid at latitude (south or north) φ is:

$$g_T = \frac{g_e(1+k\sin^2\varphi)}{(1-e^2\sin^2\varphi)^{1/2}} \qquad \textbf{(1)}$$

, where the GRS80 reference ellipsoid has the value ge = 978032.67715 mGal, being g_e the normal gravity at the equator; k = 0.001931851353 a derived constant; and e^2 = 0.0066943800229, being e the first numerical eccentricity.

The height correction, called the free-air correction, is based on the elevation (or orthometric height) above the geoid (sea level) rather than the height above the ellipsoid. The revised standards use the ellipsoid as the vertical datum rather than sea level. Conventionally, the first-order approximation formula of Δgh in mGal, or 0.3086 h, is used for this correction.

The Bouguer correction accounts for the gravitational attraction of a layer of the earth between the vertical datum, i.e., the ellipsoid, and the station. This correction, ΔgB in mGal, traditionally is calculated assuming that the earth between the vertical datum and the station can be represented by an infinite horizontal slab with the equation:

$$\Delta gB = 2\pi G\sigma h = 4,193\ x\ 10^{-5}\sigma h, \qquad (2)$$

where G, the gravitational constant, is $6.673 \pm 0.001 \times 10^{-11}$ m^3 $kg^{-1}s^{-2}$ (Mohr and Taylor, 2001) and σ is the density of the horizontal slab in kilograms per cubic meter. Additionally, the mean density is 2.67 g/cm^3 (Hinze, 2003), and h is the height of the station in meters relative to the ellipsoid in the revised procedure or relative to sea level in the conventional procedure.

The terrain correction adjusts the gravity effect produced by a mass excess (mountain) or deficit (valley) with respect to the elevation of the observation point. The terrain correction was obtained using two digital elevation models, a local one and a regional one, obtained from the Shuttle Radar Topography Mission (SRTM) of the United States Geological Survey (USGS). The software used (OASIS montaj 7.2) combines the algorithms developed by Kane (1962) and Nagy (1966). Through the use of a sampling procedure, a corresponding topographic correction value was assigned to each gravity station. The resulting maximum error for this correction was ± 1.8 mGal. Finally the complete Bouguer anomaly values (Fig. 6a) were calculated on a regular grid cell size of 5 x 5 km, using the Minimum Curvature method (Briggs, 1974).

Figure 6: *a) Bouguer anomaly map with topographic correction obtained from terrestrial data; b) crust – mantle interface depth corresponding to the hydrostatic Moho geometry calculated for the study area considering Tn = 35km; c) isostatic residual anomalies obtained from the Airy-Heiskanen compensation model; d) decompensative isostatic residual anomalies, obtained by subtracting from the isostatic anomaly an upward continuation at 35 km (Cordell et al., 1991). This anomaly shows only the gravity effects of bodies emplaced in the upper crust, since deeper effects (crustal roots) were eliminated.*

Flexural compensation models proposed by Watts (1995), Wienecke et al., (2007), Tassara et al., (2007), Pérez-Gussinyé et al., (2008), Tassara and Echaurren (2012), Álvarez et al., (2013), applied to the Central Andes have enabled the determination of elastic thicknesses which are progressively higher eastwards into the foreland zone. However, relatively low values of the effective elastic thickness next to the areas of higher crustal thickening and prolonged locus of magmatism in the Central Andes (Introcaso et al., 1992) justify the use of a "local" compensation model (Airy-Heiskanen) to evaluate the gravity field, such as in the study area, where the arc has stayed for more than 30 My and the Moho is higher than 50 km. Additionally, this model has been used in this region by several authors with the aim of eliminating negative effects of the Andean roots in order to analyze the upper crust heterogeneities (Götze and Evans 1979; Introcaso et al., 1992; Chapin 1996; Götze and Kirchner 1997; Whitman et al., 1999; Introcaso et al., 2000; Gimenez et al., 2001; Tassara and Yáñez 2003, Sánchez et al., 2015).

Previous gravity and seismic models were taken into consideration to estimate the isostatic mountain roots responding to the Airy – Heiskanen model (Martinez et al., 2006, Gimenez et al., 2009, Gans et al., 2011, Assumpção et al., 2013). Then, in this model we considered a) a normal thickness of the crust of 35 km (Tn), b) a density contrast of 0.4 g/cm^3 ($\Delta\rho$) , and c) a crust density of 2.67 g/cm^3 (ρ). The resulting hydrostatic Moho depth is shown in Figure 6b, yielding broad sectors over 50 km, and reaching locally 60 km. Then, the isostatic gravity root effect is calculated from this hydrostatic Moho geometry, obtaining the isostatic residual anomaly by subtracting this effect to the Bouguer anomaly (Figure 6c).

Therefore, the isostatic corrections could be used to remove at least partially the gravimetric effect of the crustal roots. However, they do not solve the problem when cortical roots are related to high density regions with or without topographic expression. Moreover, these anomalies can be masking other disturbances of short wavelength, generated by shallower sources (Simpson et al., 1986). To overcome this disadvantage, we performed the decompensative gravity anomaly, as proposed by Cordell et al. (1991).

Under a hypothesis of local (instead of regional) compensation, the gravity effect of a shallow geological body can be separated from the effect of its deeper compensating root inferred by deconvolution. The decompensative anomaly is the Bouguer gravity anomaly with isostatic and decompensative corrections added. Cordell et al. (1991) have proposed for this method, to perform an "upward continuation" to the isostatic anomaly (IA) in order to reduce the effect of short wavelength structures. Then, the "decompensative" anomaly (like a residual anomaly) is calculated by subtracting the upward continuation from the isostatic anomaly (Figure 6d). This anomaly signals in the foreland region broad areas that are next to isostatic equilibrium, while around the drainage divide area some areas appear in a slightly not compensated state.

Magnetic data

The magnetic database used in this work comes from different sources: i) A terrestrial dataset that is only used as a control tool to unify ii) aerial data from two aeromagnetic surveys (Argentinean Mining Geological Service, SEGEMAR). The first aerial survey was previously used in Litvak et al. (2005) (Area 9), composed of Total Magnetic Field (TMF). This was digitized and regularized using the terrestrial data as datum.

As already known, the observed value at a point of the geomagnetic field includes the contribution of the Normal Field of internal origin (about 95% of Earth's magnetic field), the Crustal Field (constituting approximately 5% of the Earth's magnetic field) and the external sources (due to the Sun – Earth interaction). These contributions are present on the value of the magnetic field measured at each point. Thus, in order to analyze the crustal magnetic field, the effects of the Normal Field and Diurnal Variations must be removed from the measured data (Dobrin, 1976). Thus, the database of the total magnetic field (TMF) was digitized and corrected by the daily variation for its corresponding time of acquisition. Such reductions were made by both companies that acquired the data and for the Instituto Volponi itself, where the data repository is placed. The Normal field is obtained from the International Geomagnetic Reference Field (IGRF), under the Responsibility of the International Association of Geomagnetisms and Aeronomy (IAGA) and the International Union of Geodesy and Geophysics (IUGS). The IGRF model is a set of Gauss coefficients and their secular variations, of degree and order from $n = m = 1$ to 10, largely representing the terms of lower degree the main field from the outer core (Hinze et al., 2013). By subtracting the IGRF values to the measured data, previously corrected for diurnal variation, the Magnetic Anomaly is obtained (Figure 7), which represents the magnetic field of crustal origin (Blakely, 1995).

Figure 7: *Magnetic Anomalies obtained from aerial and terrestrial data sets gridded in 1000 x 1000 m cells from the Minimum Curvature method (Briggs, 1974).*

Reduction to pole (RTP) (Baranov, 1975; Phillips, 2007) is a process applied to magnetic data that removes the asymmetry caused by the non-vertical direction of magnetization. The RTP method takes the total-observed magnetic field transforming it, producing a map that would have resulted considering the area in the terrestrial magnetic pole (magnetic inclination 90°). Assuming that the entire observed magnetic field is due to the induced magnetic effects, the application of this technique facilitates direct comparison with gravimetric data using the Poisson's theorem (Poisson, 1826). Such theorem states that all properties of the magnetic field due to a homogeneous body are derivable from its gravity field and vice versa. A pseudo anomaly refers to an anomaly of one type (i.e. gravity or magnetic) that has been transformed from the equivalent anomaly of the other type (i.e. magnetic or gravity) via Poisson's theorem (Hinze et al., 2013). Given an observation point placed at a distance r from the source with constant density σ and magnetization with intensity J and direction i, the Poisson's theorem connects the gravity T(r) and magnetic V(r) potentials by:

$$V(r) = \frac{J}{G\sigma}\left[\frac{\partial T(r)}{\partial i}\right] \quad (3)$$

Hence, the magnetic potential and first derivative of the gravitational potential in the direction of magnetization are linearly related by the scalar proportionality (J/Gσ). For induced magnetization at the geomagnetic field poles where $i = z$, the vertical magnetic field component Bz (or RTP) can be related to the gradient Tzz cited above. Thus,

$$RTP \cong -\frac{J}{G\sigma} T_{zz} \qquad (4)$$

Comparing pseudomagnetic and gravity effects against the respectively surveyed magnetic or gravity effects, one can test and relate the effects to a common source and reducing interpretational ambiguities (Hinze et al., 2013) (Figure 7). The result is contrasted in Figure 8 with the vertical gravity gradient obtained from Geopotential Model EGM2008, according to Poisson's equation.

Some morphostructural systems where the RTP presents morphological correspondence with the derivative of the Bouguer anomaly are the Sierra de Umango, Sierra de la Punilla and Sierra de Maz indicated on figure 8. This behavior is also observed for the northern sector of the Precordillera, in some plutons of the Colangüil batholith over the Frontal Cordillera and westwards over some places of the Chilean high Andes.

The lack of adjustment in some other places indicates that the assumption of non-existent remnant magnetization is not valid for the whole area, indicating that there is residual magnetism in some isolated sectors.

Furthermore, the RTP filter is strongly affected at low latitudes, reason by which these data were not used for subsequent modeling (MacLeod et al., 1993; Li, 2007).

Figure 8: *Comparison between the Reduced to Pole Magnetic Anomaly vs. Vertical Gravity Gradient, from the application of the Poisson´s theorem, as an independent test to avoid sectors with remnant magnetization in the interpretation of basin geometry and modeling.*

Analysis

3D Gravity Inversion and determination of the basement depth

An inversion method has been applied based on obtaining the Fourier transform of the gravitational effect, integrated into a $z = z_0$ plane passing through a point $P\ (x,y)$ located at a certain distance, in order to produce a 3D map of the basement geometry in the study area (Figure 9) (Chai and Hinze, 1988; Guspi, 1992; Chakravarthi, 2001). The software used for modeling operates in frequency domain and is based on the algorithm of Parker (1972). This algorithm consists in obtaining the Fourier transform of the potential field, expressed as an infinite strongly convergent Fourier transform series, whose expression is

$$\hat{g}_0 = (\bar{k}) = 2\pi G \exp(kz_0)\, x \sum_{n=1}^{\infty} \frac{(-k)^{n-1}}{(n-1)!} F \left[\sum_{j=0}^{m} \frac{a_j(\bar{r})\, h^{n+j}(\bar{r})}{n+j}\right] \quad (5)$$

, and where G is the universal gravitational constant; i, an imaginary unit; k, $\bar{k}$ vector module, n the polynomial degree; and F the Fourier transform. The result given by Parker (1972) corresponds to a polynomial of 0 degree, and a polynomial of 1 degree with constant coefficients, which leads to the formula of Reamer and Ferguson (1989). This result can be extended to multiple layering and variable density with position.

In order to approximate the depth of the basement interface, an inversion was calculated using GMSYS 3D® software for each stratum defined by grids located in one half-space (Parker, 1972). For correct data processing, grids must be expanded in order to eliminate border effects (Blakely, 1995). In this case, we used a 20% expansion of the grid, and grid spacing of 1000 m between nodes. The model uses the residual gravity anomalies shown in Figure 5d as data entry, where deep components were filtered. In order to compute the depth of the crystalline basement and therefore the geometry of the Cenozoic basins, the program takes as input parameter the density distribution at depth. Therefore, this basement inversion model (Figure 9) is performed assuming a 3 layer model with stratified density values. The shallower layer corresponds to the sedimentary infill with a mean density of 2.4 g/cm^3, representing mostly Quaternary unconsolidated sediments; while a deeper medium represents the Cenozoic sequences with a mean density of 2.68 g/cm^3 and finally the deepest layer represents a Permian - Triassic basement with a density of 2.88 g/cm^3.

This three-layer model provides a first order approximation of the geometry and depth of the basement across the highest Andes in the northern Chilean-Pampean flat slab region. Figure 9 shows a general interpretation of such basement topography which outlines major sedimentary depocentres. This scheme signals the approximate depth and exact geometry of some already known depocenters (foreland depocenters located at the eastern Andean front;

e.g. Matagusanos, Tulum, Bermejo, Vinchina depocenters, and others incorporated into the orogenic wedge, e.g. Iglesia-Calingasta depocenter), while also indicate the existence of others not described previously, particularly those located at the highest Andes around the drainage divide area and buried by thick sections of Cenozoic strata. These depocenters are interpreted as associated with syn-extensional topography produced during the Doña Ana extensional stage that affected the Andes at these latitudes. Thus, this model is used as an initial framework to perform an improved and more detailed bi-dimensional model across 29º30' S, using additional geological and geophysical constraints.

Figure 9: *Basement depth computed from gravity inversion. Note how foreland basins are defined as elongated lows parallel to the mountain fronts, delineated by gravity highs, and how the Frontal Cordillera basement is characterized by more equidimensional lows and highs that are potentially associated with the synextensional topography produced during Doña Ana basin development (see text or further details). Interrupted line formed by points and short traces indicates the Chilean-Argentinean boundary as a reference. Thinner interrupted lines are Province and District boundaries as a reference.*

Figure 10: *Below: 3D perspective of the computed basement depth, obtained from inversion of gravity data (see text for details), with underlying Nazca subducted slab geometry obtained from seismic data and Moho geometry obtained from gravity data (see previous sections). A digital terrain model grid (DEM 90 x 90m) is indicated above as a reference.*

Gravity and magnetic 2D inversion

Two direct 2D models were traced at 29°30' S after obtaining the results of the 3D inversion depth basement. For these direct models the GM-SYS 2D software developed by Webring (1985) was used (see Figures 1 and 3 for location). This software is based on methods implemented by Talwani et al. (1959) and improved by Marquardt (1963) algorithm. One of the models, modeled from the complete Bouguer anomaly, has been designed for regional purposes, particularly to delineate crustal heterogeneities, while the other was more local, modeling the residual Bouguer anomaly, in order to only constraint upper crustal structures.

For the lithospheric (whole crust)-scale 2D model, blocks representing the upper mantle with density $\rho_m = 3.41\ g/cm^3$, Nazca Plate with density $\rho_{nz} = 3.05 - 3.1\ g/cm^3$, subduction channel with density $\rho_{sc} = 2.9\ g/cm^3$, and South American lower crust with density $\rho_{lc} = 2.85\ g/cm^3$, mid crust with density $\rho_{mc} = 2.7\ g/cm^3$, and upper crust with density $\rho_s = 2.67\ g/cm^3$, were considered. Mafic rocks trapped at the potential suture zones between the different proposed Paleozoic terranes cited in literature were modeled with densities $\rho_{sut} = 2.95 \text{ to } 3.00\ \mathrm{g/cm^3}$ (see Gimenez et al., 2009 and references therein).

Additionally, this model includes lateral density variations through the Nazca plate, produced by dehydration and densification at depth (Pacino and Introcaso 1988). The geometry of the Nazca plate at depth is adjusted in the model using a catalog of 213 interplate earthquakes (http://www.isc.ac.uk/ehbbulletin/search/catalogue/), filtering the Mw≥4 events.

The complete Bouguer Anomaly corrected for height (Figure 6a) was used for this model, in which the long wavelengths were adjusted considering lateral variations in density through mid and lower crust (Figure 11).

In order to adjust the model, lateral density variations were introduced considering proposals that determine basement heterogeneity associated with accretional micro-continental phases (see Gimenez et al., 2009 and references therein), with Pampia basement with a density of 2.72 g/cm^3, Cuyania with 2.64 to 2.70 g/cm^3, Chilenia with 2.82 g/cm^3, and an extra heterogeneous region to the west potentially considered as a different hypothetical basement block with a density of 2,80 g/cm^3.

***Figure 11:** a) Lithospheric model across 29° 30'S adjusted using the complete Bouguer anomaly. Mafic rocks are included in the areas of potential sutures between different Paleozoic terranes already implemented in Gimenez et al., (2009). Note that while limits between the different basements of Frontal Cordillera, Precordillera and western Sierras Pampeanas have been linked to Paleozoic sutures, the westernmost discontinuity included in this model does not follow any previous proposal.*

For the local-upper crustal model (Figure 12), the densities used are the ones already introduced in the three-dimensional inversion, as well as the general geometry of the basement at depth. Therefore sedimentary Quaternary infill was modeled using a range of density values between 2.3 and 2.4 g/cm^3, being typical values of sedimentary sections in the area (Gimenez et al., 2000; Ruiz and Introcaso, 2000; Introcaso et al., 2004).

The deepest sedimentary (volcanoclastic and clastic) units and the crystalline basement were modeled with densities ranging from 2.6 to 2.88 g/cm^3, including Carboniferous and lower Paleozoic, Permo-Triassic, Cretaceous and Cenozoic sections. These density vales were already used for other neighbor crustal models in Sierras Pampeanas and Precordillera areas (Martinez and Gimenez, 2003; Kostadinoff et al., 2010).

Mafic high density rocks were modeled delineating the Cuyania and Pampia terrane boundary zone inferred across the Valle Fertil Lineament (Gimenez et al., 2000; Ruiz and Introcaso, 2000; Martinez and Gimenez, 2003), using the same density values for the regional model (ρ = 2.72 g /cm^3).

Furthermore, to adjust this profile, magnetic susceptibility values, obtained by reversing the magnetic field, were used (Figure 7). These data were corroborated by susceptibility values sampled in the outcrops that are consistent with standard values for different rock types (Telford et al., 1990; Chernicoff et al., 2009; Kostadinoff et al., 2010).

Figure 12: *a) Structural cross section based on Winocur et al., (2015) (geological data displayed on figures 3 and 4) across -29° 30' S and adjusted from gravity and magnetic data.*

Discussion

Gravity and magnetic data have allowed delineating a series of anomalies interpreted as depocenters in the Frontal Cordillera area of the northern Chilean-Pampean flat slab segment of the Southern Central Andes. These data are valuable in understanding basin architecture and Mesozoic to Paleogene structure since extensive blankets of volcanic strata of the Permian-Triassic Choiyoi Group, and the Eocene-Miocene Doña Ana and Farellones formations characterize the highest Andes, burying most of the basement structure. This particular array of lows suggests the presence of kilometer-scale depocenters on both sides of the high Andes separated by NW transfer zones (Figures 9 and 10) that coincide with exposures of the Permian-Triassic Choiyoi Group and Eocene-early Miocene Doña Ana Formation, both units considered, in a vast part of literature, synrift associations linked to two periods of crustal stretching, one during Pangea break-up and a younger during the extensional destabilization of an Incaic relief mostly developed on the Chilean side of the Andes. 2D regional gravity models that adjust the measured gravity data and more locally gravity and magnetic profiles (Figures 11 and 12) imply the presence of a different crustal basement block on the Chilean slope of the Andes separated by an east-dipping discontinuity. This geometry could explain the development of Mesozoic?-Paleogene depocenters in the present Andean drainage zone as a result of the extensional collapse of the hanging wall of a hypothetical suture (Figure 13), constrained on gravity criteria, whose real nature needs further geological analyses. Then the structure of the Frontal Cordillera, partly derived from inversion of these depocenters could also be the result of the reactivation of a crustal-scale discontinuity explaining its deep decollement.

Figure 13: *Schematic representation of the Paleogene extensional setting in the Southern Central Andes and the reactivation of a potential crustal heterogeneity inferred from gravity modeling.*

Conclusions

The 3D and 2D models constructed from the decompensative gravity and magnetic anomalies adjusted with the available geological and geophysical information (Ramos et al., 2002; Gimenez et al., 2009; Winocur et al., 2015, among others) revealed the geometry of the basement in a sector of the high Andes placed in the northern Chilean-Pampean flat subduction segment. In this model, elongated depocenters, associated with the eastern and western deformational fronts of Precordillera and Sierras Pampeanas respectively at the eastern deformational front of the Andes, are coincident with Neogene foreland basins. However, a mosaic of equidimensional smaller depocenters appears at the Frontal Cordillera area at both sides of the high Andes, interpreted as a result of the synextensional topography of the Doña Ana Basin developed in Eocene to late Oligocene times. The lithospheric-scale 2D model suggests the presence of a non-previously recognized crustal discontinuity to the west of these depocenters corresponding to the Doña Ana Basin that could have hypothetically exerted a control on focalizing extension (Figure 13). This newly proposed basement discontinuity, summed to the ones recognized in the model potentially associated with the amalgamation of Cuyania and Pampean allochtonous, should be taken into consideration for further Paleozoic plate reconstructions, analyzing potential times of docking and associated deformational processes on geological grounds.

Acknowledgements

The authors acknowledge the use of the GMT-mapping software of Wessel & Smith (1998). We are also grateful to YPF S.A. company for access to data by Project FSTics 2010 nº0006, CAPP-Ondas, Team 1 – Seismology, Universidad Nacional de San Juan, FONARSEC. FONCYT 2012 – 2716, CICITCA 21E905.

References

Anderson, E. G., 1976. The effect of topography on solutions of Stokes' problem. Unisurv S-14, Rep, School of Surveying, University of New South Wales, Kensington.

Álvarez, O., Gimenez, M. E., Braitenberg, C., Folguera, A., 2012. GOCE satellite derived gravity and gravity gradient corrected for topographic effect in the South Central Andes region. Geophysical Journal International 190 (2), 941–959.

Álvarez, O., Giménez, M., Braitenberg, C., 2013. Nueva metodología para el cálculo del efecto topográfico para la corrección de datos satelitales. Revista de la Asociación Geologica Argentina 70 (4), 422-429.

Assumpção, M., Bianchi, M., Julià, J, Dias, F., Sand França, G., Nascimento, R., Drouet, S., Garcia Pavão, C., Farrapo Albuquerque, D., Lopes, A. E.V., 2013. Crustal thickness map of Brazil: Data compilation and main features. Journal of South American Earth Sciences 43, 74 -85.

Baldis, B. A., Beresi, M., Bordonaro, L., Vaca, A., 1982. Síntesis evolutiva de La Precordillera Argentina. 5º Congreso Latinoamericano de Geología, Actas 4, pp. 399-445.

Baranov, V., 1975. Potential fields and their transformations in applied geophysics. Geoexploration Monograph, Series L, 6: Gerbruder Borntraeger, Berlin, Stuttgart, Germany.

Barthelmes, F., 2009. Definition of functionals of the geopotential and their calculation from spherical harmonic models theory and formulas used by the calculation service of the International Centre for Global Earth Models (ICGEM). Scientific Technical Report STR09/02, GFZ German Research Centre for Geosciences, Postdam, Germany. http://icgem.gfz-postdam.de

Bissig, T., Clark, A. H., Lee, J. K. W., Heather, K. B., 2001. The Cenozoic history of volcanism and hydrothermal alteration in the Central Andean flat-slab region: New 40Ar-39Ar constrains from the El Indio-Pascua Au-(Ag, Cu) belt, 29°20´-30°30´ S. International Geology Review 43, 312-340.

Blakely, R. J., 1995. Potential theory in gravity and magnetic applications. Cambridge University Press, 441 New York.

Briggs, I. C., 1974. Machine contouring using minimum curvature. Geophysics 39 (1), 39-40.

Caminos, R. and Fauqué, L., 2001. Hoja Geológica 2969-II Tinogasta, Provincia de La Rioja, 1:250.000. Instituto de Geología y Recursos Minerales, SEGEMAR.

Cardó, R., Díaz, I., Cegarra, M., Rodríguez, R., Heredia, N., Santamaría, G., 1998. Hoja Geológica 3169-I: Rodeo, escala 1: 250.000.

Cardó, R., Díaz, I. N., Poma, S., Litvak, V. D., Santamaría, G., Limarino, C. O., 2001. Memoria Hoja Geológica 2969-III, Malimán. Servicio Geológico Minero Argentino, 67.

Chai, Y., and Hinze, W. J., 1988. Gravity inversion of an interface above which the density contrast varies exponentially with depth. Geophysics 53, 837–845.

Chakravarthi, V., Singh, S. B., Ashok Babu, G., 2001. Inver2dbase — A program to compute basement depths of density interfaces above which the density contrast varies with depth. Computers & Geosciences 27 (10), 1127-1133.

Chapin, D. A., 1996. A deterministic approach toward isostatic gravity residuals-A case study from South America. Geophysics 61, 1022–1033.

Charchaflié, D., Tosdal, R. M., Mortensen, J. K., 2007. Geologic framework of the Veladero high-sulfidation epithermal deposit area, Cordillera Frontal, Argentina. Economic Geology 102, 171–192.

Charrier, R., Pinto, L., Rodriguez, M. P., 2007. Tectonostratigraphic evolution of the Andean orogen in Chile. In Geology of Chile, Chapter 3 (Gibbons, W. and Moreno,T., editors.) The Geological society of London, Special Publication, 21-116.

Chernicoff, C. J. and Nash, C. R., 2002. Geological interpretation of Landsat TM imagery and aeromagnetic survey data, northern precordillera region, Argentina. Journal of South American Earth Sciences 14, 813-820.

Chernicoff, C. J., Vujovich, G. I., Van Staal, C. R., 2009. Geophysical evidence for an extensive Pie de Palo Complex mafic–ultramafic belt, San Juan, Argentina. Journal of South American Earth Sciences 28 (4), 325-332.

Cordell, L., Zorin, Y. A., Keller, G. R., 1991. The decompensative gravity anomaly and deep structure of the region of the Rio Grande rift. Journal of Geophysical Research 96, 6557–6568.

Dobrin, M., 1976. Introduction to geophysical prospecting. McGraw Hill, 3rd edition, pp. 630.

Farías, M., 2007. Tectonique, Erosion Et Evolution Du Relief Dans Les Andes Du Chili Central Au Cours Du Neogene. Tesis Doctoral.

Fauqué, L. E., Limarino, C. O., Vujovich, G. I., Cegarra, M., Escosteguy, L., 2002. Hoja Geológica 2969-IV Villa Unión, Provincias de La Rioja y San Juan.

Fauqué, L., 2010. Memoria Hoja Geológica 2969-I, Pastillos. Servicio Geológico Minero Argentino.

Furque, G., González, P., Caballé, M., 1998. Descripción de la hoja geológica 3169-II, San José de Jáchal (Provincias de San Juan y La Rioja). Servicio Geológico Minero Argentino, Boletín, 259.

Gans, C. R., Beck, S. L., Zandt, G., Gilbert, H., Alvarado, P., Anderson, M., Linkimer, L., 2011. Continental and oceanic crustal structure of the Pampean flat slab region, western Argentina, using receiver function analysis: new high-resolution results. Geophysical Journal International 186, 45–58.

Gimenez, M. E., Martinez, M. P., Introcaso A., 2000. A crustal model based mainly on gravity data in the area between the Bermejo Basin and the Sierras de Valle Fértil, Argentina. Journal of South American Earth Sciences 13, 275 -286.

Gimenez, M., Martinez, M. P., Introcaso, A., 2001. Análisis Hidrostático de la Cuenca del Bermejo (Provincia de San Juan- Argentina). Revista de la Asociación geológica Argentina 56 (4), 419-424.

Gimenez M., Martinez P., Jordan T., Ruiz F., Lince Klinger F., 2009, Gravity characterization of the La Rioja Valley Basin, Argentina. Geophysics 74 (3), B83-B94.

Götze, C., and Evans, B., 1979. Stress and temperature in the bending lithosphere as constrained by experimental rock mechanism. Geophysical Journal of the Royal Astronomical Society 59, 463–478.

Götze, H. J., and Kirchner, A., 1997. Interpretation of gravity and geoid in the Central Andes between 20° and 29° S. Journal of South American Earth Sciences 10, 179–188.

Guspí, F., 1992. Three-dimensional Fourier gravity inversion with arbitrary density contrast: Geophysics 57, 131–135.

Hinze, W. J., von Frese, R. B., Saad, A. H., 2013. Gravity and Magnetic Exploration. Principles, Practices, and Applications. Published in the United States of America by Cambridge University Press, New York. ISBN 978-0-521-87101-3 Hardback.

Introcaso, A., Guspí, F., Robles, A., Martinez, P., Miranda, S., 1992. Carta gravimétrica de Precordillera y Sierras Pampeanas entre 30° y 32° de Latitud Sur. Actas Reunión de la Asociación Argentina de Geofísicos y Geodestas, Buenos Aires, pp. 178.

Introcaso, A., Pacino, M. C., Guspi, F., 2000. The Andes of Argentina and Chile: Crustal configuration, Isostasy, Shortening and Tectonic features from Gravity Data. Temas de Geociencia 5, 31.

Introcaso, A., Martinez, M. P., Gimenez, M., Ruiz, F., 2004. Geophysical Study of the Valle Fértil Lineament Between 28º 45' S and 31º 30' S: Boundary Between the Cuyania and Pampia Terranes. Gondwana Research. Special Ed. “Cuyania, an exotic block to Gondwana” 7 (4), 1117-1132.

Kane, M. F., 1962. A comprehensive system of terrain corrections using a digital computer. Geophysics, 27(4), 455-462.

Kostadinoff, J., Ferracutti, G. R., Bjerg, E. A., 2010. Interpretación de una sección gravi magnetométrica sobre la Pampa de las Invernadas, Sierra Grande de San Luis. Revista de la Asociación Geológica Argentina 67, 349 - 353.

Li, X., 2007. Magnetic reduction-to-the-pole at low latitudes: Practical considerations. In 2007 SEG Annual Meeting. Society of Exploration Geophysicists.

Litvak, V. D., Chernicoff, C. J., Poma, S. M., 2005. Localización de centros eruptivos mediante areomagnetometría en el sector central del Valle del Cura, San Juan, Argentina: implicancias para la evolución del arco/retroarco cenozoico. Revista Geológica de Chile 32(1), 77-93.

Litvak, V. D., 2009. El volcanismo Oligoceno superior – Mioceno inferior del Grupo Doña Ana en la Alta Cordillera de San Juan. Revista de la Asociación Geológica Argentina, 64(2), 201-213.

Llambias, E. J., and Sato, A. M., 1990. El Batolito de Colangüil (29-31°S) cordillera frontal de Argentina: estructura y marco tectonico. Andean Geology,17(1), 89-108.

MacLeod, I. N., Jones, K., Dai, T. F., 1993. 3-D analytic signal in the interpretation of total magnetic field data at low magnetic latitudes. Exploration Geophysics, 24(3/4), 679-688.

Maksaev, V., Moscoso, R., Mpodozis, C., Nasi, C., 1984. Las unidades volcánicas y plutónicas del Cenozoico superior en la Alta Cordillera del Norte Chico (29°-31°S), Geología, alteración hidrotermal y mineralización. Revista Geológica de Chile 21, 11-51.

Marín, G., y Nullo, F., 1989. Geología y estructura del oeste de la Cordillera de la Ortiga, San Juan. Revista de la Asociación Geológica Argentina 43(2), 153-163.

Marquardt, D. W., 1963. An algorithm for least-squares estimation of nonlinear parameters. Journal of the Society for Industrial & Applied Mathematics 11(2), 431-441.

Martin, M.W., Clavero, J., Mpodozis, C., Cuitiño, L., 1995 Estudio Geológico de la Franja El Indio, Cordillera de Coquimbo: Servicio Nacional de Geología y Minería, Informe Registrado IR-95-6 (1), 1-238, Santiago.

Martinez, M. P., Gimenez M. E., 2003. Fuerte anomalía gravimétrica residual positiva en el Sistema de Famatina y su relación con paleosuturas. Explicaciones alternativas. Revista de la Asociación Geológica Argentina 58(2), 176-186.

Martinez, M. P., Gimenez, M. E., Bustos, G., Lince Klinger, F., Mallea, M., Jordan, T. J., 2006. Detección de saltos de basamento de la cuenca del valle de La Rioja - Argentina a partir de un modelo hidrostático. GEOACTA, 31 1 - 9.

Martínez, F., Arriagada, C., Valdivia, R., Deckart, K., Peña, M., 2015. Geometry and kinematics of the Andean thick-skinned thrust systems: Insights from the Chilean Frontal Cordillera (28°–28.5° S), Central Andes. Journal of South American Earth Sciences, 64, 307-324.

Mayer-Gürr, T., 2007. ITG-GRACE03S: the latest GRACE gravity field solution computed in Bonn. Joint International GSTM and DFG SPP symposium. October 2007, Potsdam.

Molodensky, M.S., Eremeev, V.F., Yurkina, M.I., 1962. Methods for study of the external gravity field and figure of the earth. Israel Program of Scientific Translations, pp. 248.

Mohr, P. J., and Taylor, B. N., 2001. Adjusting the values of the fundamental constants.

Moritz, H., 1980. Advanced physical geodesy. Advances in Planetary Geology, 1.

Mpodozis, C. and Ramos, V. A., 1989. The Andes of Chile and Argentina. In Ericksen, G.E., Cañas Pinochet, M.T. and Reinemud, J.A., (Eds.). Geology of the Andes and its relation to hydrocarbon and mineral resources, Circumpacific Council for Energy and Mineral Resources, Earth Sciences Series 11, 59-90.

Mulcahy, P., Chen, C., Kay, S. M., Brown, L. D., Isacks, B. L., Sandvol, E., Heit, B., Chen, Y., Coira, B. L., 2014. Central Andean mantle and crustal seismicity beneath the Southern Puna plateau and the northern margin of the Chilean-Pampean flat slab. Tectonics 33, 1636-1658.

Nagy, D., 1966. The gravitational attraction of a right rectangular prism. Geophysics, 31(2), 362-371.

Nullo, F., 1988. Geología y estructura del área de Guanaco Zonzo y Veladero, oeste de la Cordillera de Zancarrón, San Juan. 3° Congreso Nacional de Geología Económica, Olavarría. Actas 2, pp. 501-515.

Pacino, M. C., Introcaso, A., 1988. Modelo gravimétrico sobre el sistema de subducción Placa de Nazca Sudamericana en la latitud 33° Sur. V Congreso Geológico Chileno, Actas (T2), pp. 77-89.

Parker, R. L., 1972. The rapid calculation of potential anomalies. Geophysical Journal of the Royal Astronomical Society 31, 447-455.

Pavlis, N. K., Holmes, S. A., Kenyon, S. C., Factor, J. K., 2012. The development and evaluation of the Earth Gravitational Model 2008. Journal of Geophysical Research 117, 404 -406.

Phillips, J. D., Hansen, R. O., Blakely, R. J., 2007. The use of curvature in potential-field interpretation. Exploration Geophysics 38(2), 111-119.

Pérez-Gussinyé , M., Lowry, A. R., Phipps Morgan, J., Tassara, A., 2008. Effective elastic thickness variations along the Andean margin and their relationship to subduction geometry. Geochemistry Geophysics Geosystems 9(2). http://dx.doi.org/10.1029/2007GC001786

Poisson, S. D., 1826. Memoire sur la theorie du magnetisme. Memories de la l'acadamie royale des sciences de l'Institute de France, Paris.

Ramos, V. A., Jordan, T. E., Allmendinger, R., Mpodozis, C., Kay, S. M., Cortes, J. M., Palma, M., 1986. Paleozoic terranes of the Central Argentine-Chilean Andes. Tectonics 5, 855–880.

Ramos, V. A., Page, R., Kay, S. M., Lapido, O. Delpino, D., 1987. Geología de la región del volcán Tórtolas, valle del Cura, provincia de San Juan. 10° Congreso Geológico Argentino and Simposium of Circumpacific Phanerozoic Granites, Tucumán. Actas 4: pp. 260-263.

Ramos, V. A., Cristallini, E. O., Pérez, D. J., 2002. The Pampean flat-slab of the Central Andes. Journal of Southamerican Earth Sciences 15, 59-78.

Reamer, S K., and Ferguson, J. F., 1989. Regularized two-dimensional Fourier gravity inversion method with application to Silent Canyon caldera, Nevada. Geophysics 54, 486-496.

Ruiz, F., Introcaso, A., 2000. La estructura profunda de la cuenca sedimentaria Ischigualasto - Villa Unión: Una interpretación tectónica a partir de datos de gravedad y magnetismo (Parte 1). UNR Editora. Temas de Geociencia (4). 70 p. Rosario.

Sánchez, M., Klinger, F. L., Martinez, M. P., Alvarez, O., Ruiz, F., Weidmann, C., Folguera, A., 2015. Geophysical characterization of the upper crust in the transitional zone between the Pampean flat slab and the normal subduction segment to the south (32-34° S): Andes of the Frontal Cordillera to the Sierras Pampeanas. Geological Society, London, Special Publications 399(1), 167-182. http://dx.doi.org/10.1144/SP399.1

Simpson, R. W., Jachens, R. C., Blakely, R. J., Saltus, R. W., 1986. A new isostatic residual gravity map of the conterminous United States with a discussion on the significance of isostatic residual anomalies. Journal of Geophysical Research: Solid Earth, 91(B8), 8348-8372.

Somigliana, C., 1930. Sul campo gravitazionale esterno del geoide ellissoidico.

Tassara, A., Swain, C., Hackney, R., Kirby, J., 2007. Elastic thickness structure of South America estimated using wavelets and satellite-derived gravity data. Earth and Planetary Science Letters, 253, 17–36.

Tassara, A. and Yáñez, G., 2003. Relación entre el espesor elástico de la litófera y la segmentación tectónica del margen andino (15-47°S). Revista Geológica de Chile 30, 159–186.

Tassara, A. and Echaurren, A., 2012. Anatomy of the Andean subduction zone: three-dimensional density model upgraded and compared against global-scale models. Geophysical Journal International 189, 161–168.

Telford, W., Geldart, L., Sheriff, R., 1990. Applied Geophysics. Cambridge University Press, Chapter 6, 293-297, Cambridge.

Thiele, R., 1964. Reconocimiento geológico de la Alta Cordillera de Elqui. Universidad de Chile, Departamento de Geología, Publicaciones, 27, 1-73. Santiago.

Vicente, J. C., 2005. Dynamic paleogeography of Jurassic Andean Basin: pattern of transgression and localization of main straits through the magmatic arc. Revista de la Asociación Geológica Argentina 15, 221-250.

Villella, J. C., and Pacino, M. C., 2010. Interpolación gravimétrica para el cálculo de los números geopotenciales de la red altimétrica de Argentina en zonas de alta montaña. Geoacta, 35(2), 13-26.

Watts, A. B., Lamb, S. H., Fairhead, J. D., Dewey, J. F., 1995. Lithospheric flexure and bending of the Central Andes. Earth and Planetary Science Letters 134, 9-20.

Webring, M., 1985. SAKI; a Fortran program for generalized linear inversion of gravity and magnetic profiles US Geological Survey 85, 122.

Weidmann, C., Spagnotto, S., Álvarez, O., Sánchez, M., Klinger, F. L., Giménez, M., Martinez, P., 2013. Crustal structure and tectonic setting of the south central Andes from gravimetric analysis. Geofísica internacional 52(3), 197-208.

Wessel, P. and Smith, W. H. F., 1998. New, improved version of the Generic Mapping Tools released, Eos Trans. AGU, 79, 579

Whitman, D., 1999. Isostatic residual gravity anomaly in the Central Andes: 12 to 29°. S: A guide to interpreting crustal structure and deeper lithospheric processes. International Geology Review 41, 457 – 475.

Wienecke, S., Braitenberg, C., Götze, H. J., 2007. A new analytical solution estimating the flexural rigidity in the Central Andes. Geophysical Journal International 169, 789–794.

Winocur, D., and Ramos, V., 2008. Geología y Estructura del sector norte de la Alta Cordillera de la provincia de San Juan. In Congreso Geológico Argentino(17), pp. 166-167.

Winocur, D., and Ramos, V., 2011. La Formación Valle del Cura: Su edad y ambiente tectónico. In 18 Congreso Geológico Argentino.

Winocur, D. A., Litvak, V. D., Ramos, V. A., 2015. Magmatic and tectonic evolution of the Oligocene Valle del Cura basin, main Andes of Argentina and Chile: evidence for generalized extension. Geological Society, London, Special Publications 399 (1), 109-130. http://dx.doi.org/10.1144/SP399.2

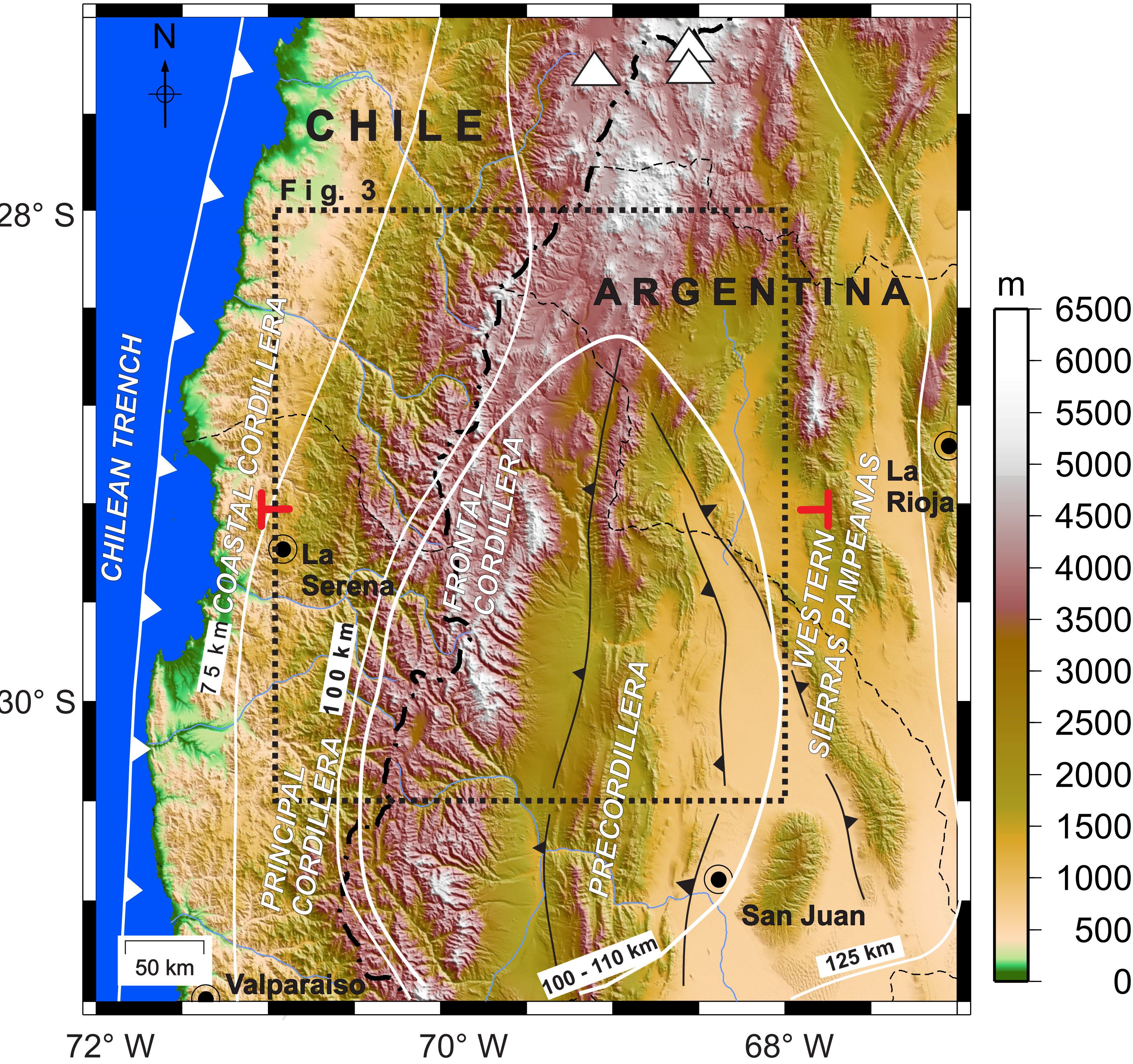

N
CHILE
Fig. 3
ARGENTINA
CHILEAN TRENCH
COASTAL CORDILLERA
FRONTAL CORDILLERA
PRINCIPAL CORDILLERA
PRECORDILLERA
WESTERN SIERRAS PAMPEANAS
La Serena
La Rioja
San Juan
Valparaiso
75 km
100 km
100 - 110 km
125 km
50 km
28° S
30° S
72° W
70° W
68° W
m
6500
6000
5500
5000
4500
4000
3500
3000
2500
2000
1500
1000
500
0

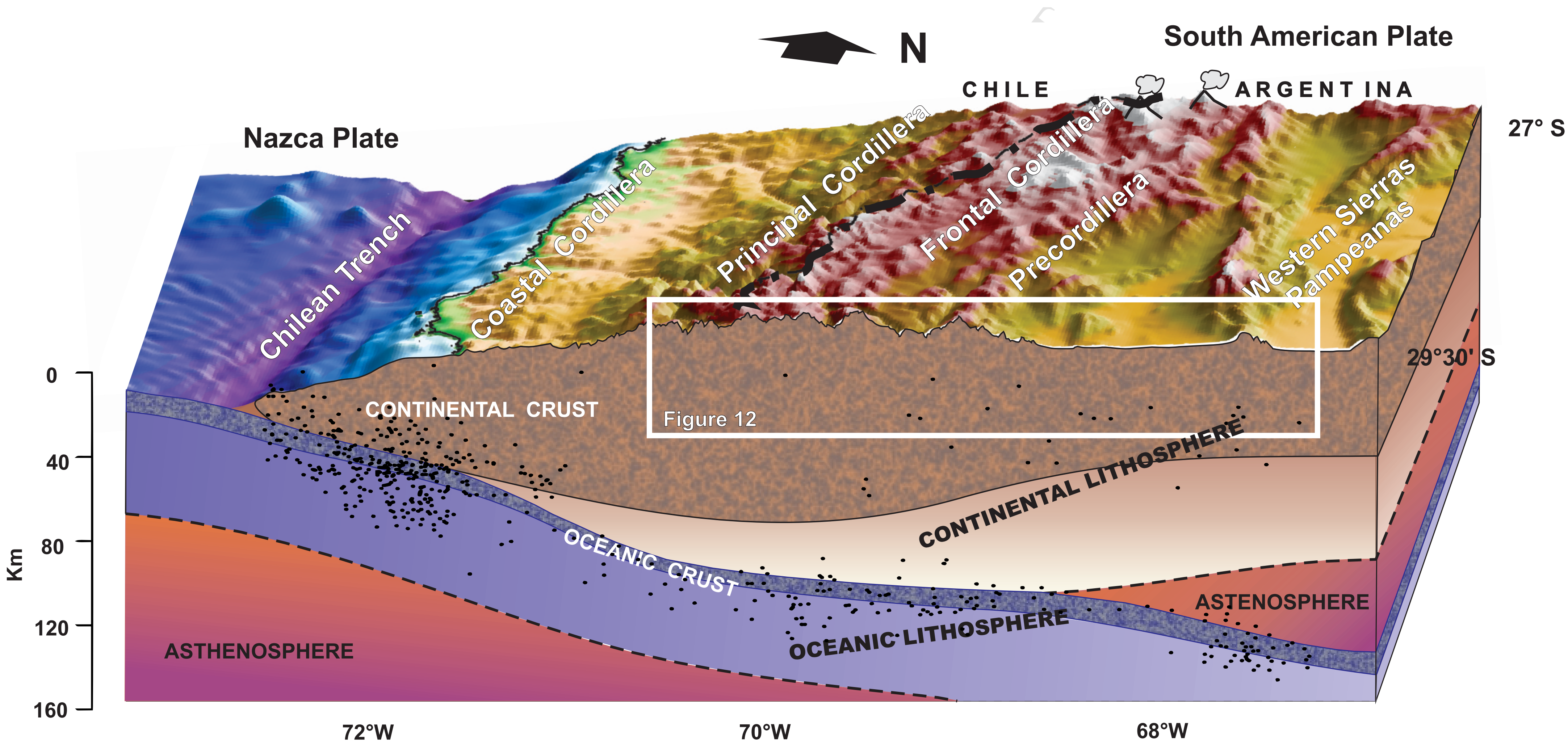
N
South American Plate
Nazca Plate
CHILE
ARGENTINA
27° S
29°30' S
Chilean Trench
Coastal Cordillera
Principal Cordillera
Frontal Cordillera
Precordillera
Western Sierras Pampeanas
Figure 12
CONTINENTAL CRUST
CONTINENTAL LITHOSPHERE
OCEANIC CRUST
OCEANIC LITHOSPHERE
ASTENOSPHERE
ASTHENOSPHERE
Km
0
40
80
120
160
72°W
70°W
68°W

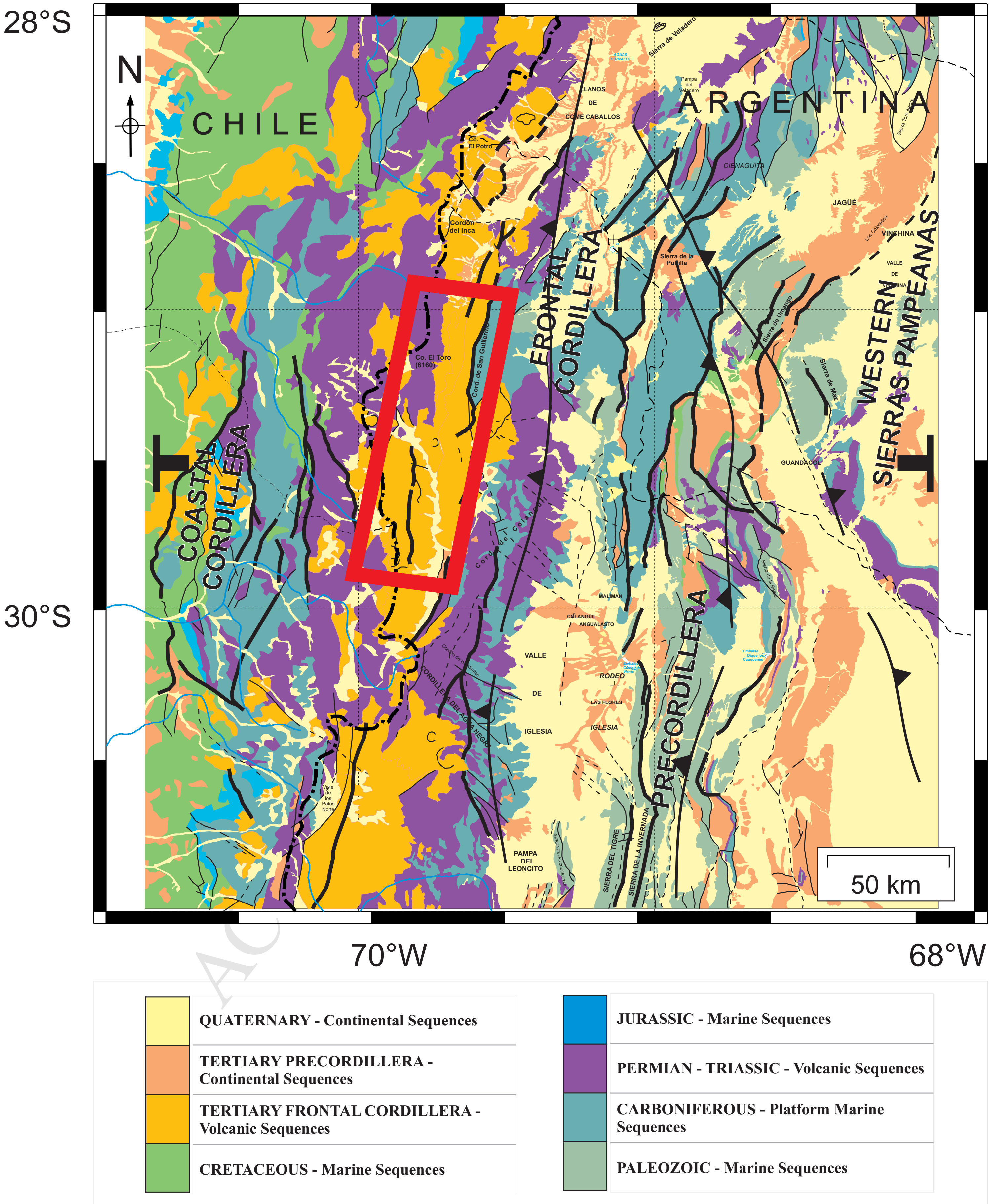
28°S
30°S
70°W
68°W
N
CHILE
ARGENTINA
COASTAL CORDILLERA
FRONTAL CORDILLERA
PRECORDILLERA
WESTERN SIERRAS PAMPEANAS
Co. El Toro (6160)
Cord. de San Guillermo
Cordón del Inca
Co. El Potro
Sierra de Veladero
LLANOS DE COME CABALLOS
CIENAGUITA
JAGÜE
VINCHINA
Sierra de la Punilla
Sierra de Umango
Sierra de Maz
GUANDACOL
VALLE DE IGLESIA
RODEO
LAS FLORES
IGLESIA
MALIMAN
COLANGUIL
ANGUALASTO
CORDILLERA DE LA AGUA NEGRA
PAMPA DEL LEONCITO
SIERRA DEL TIGRE
SIERRA DE LA INVERNADA
50 km
QUATERNARY - Continental Sequences
TERTIARY PRECORDILLERA - Continental Sequences
TERTIARY FRONTAL CORDILLERA - Volcanic Sequences
CRETACEOUS - Marine Sequences
JURASSIC - Marine Sequences
PERMIAN - TRIASSIC - Volcanic Sequences
CARBONIFEROUS - Platform Marine Sequences
PALEOZOIC - Marine Sequences

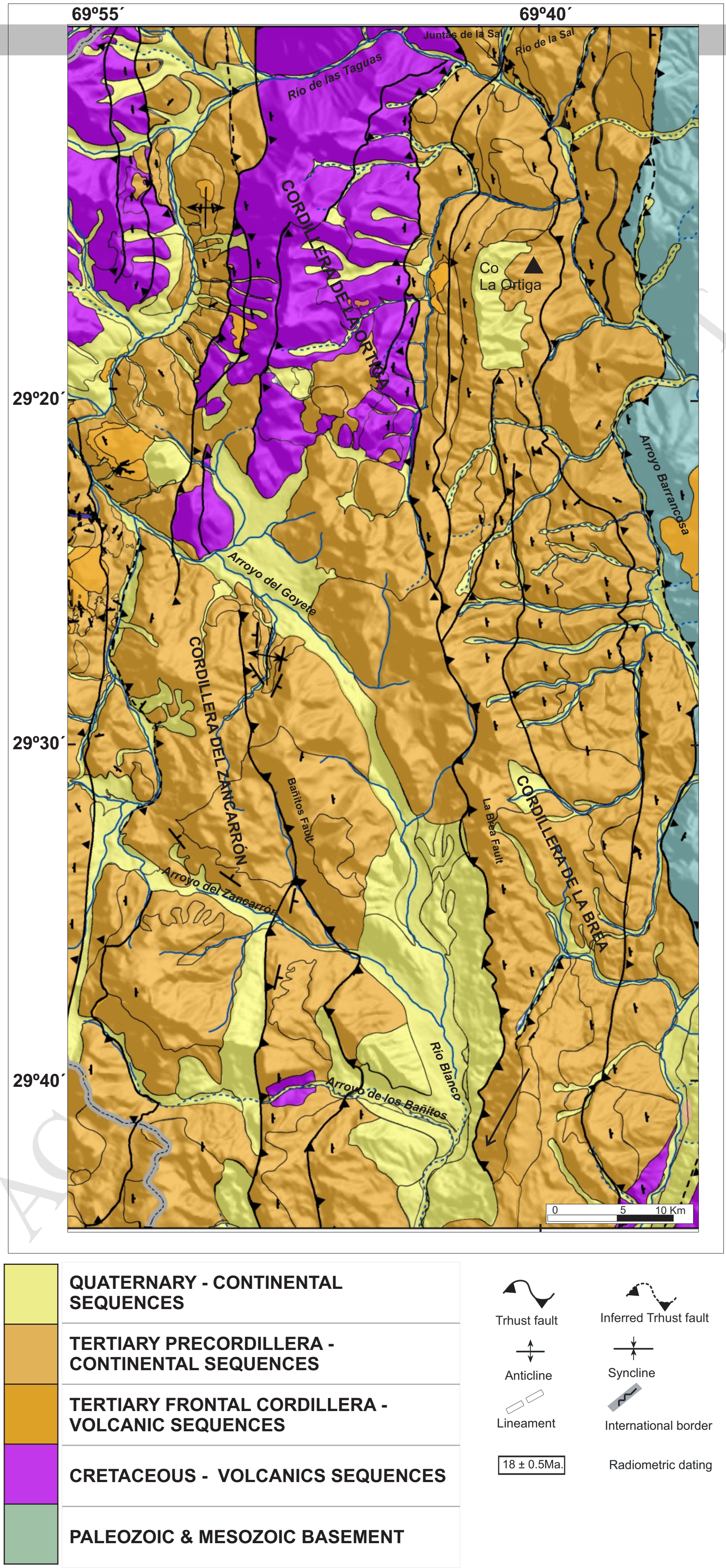

69º55´
69º40´
29º20´
29º30´
29º40´
Juntas de la Sal
Río de la Sal
Río de las Taguas
CORDILLERA DE LA ORTIGA
Co
La Ortiga
Arroyo Barrancosa
Arroyo del Goyete
CORDILLERA DEL ZANCARRÓN
Bañitos Fault
La Brea Fault
CORDILLERA DE LA BREA
Arroyo del Zancarrón
Río Blanco
Arroyo de los Bañitos
0
5
10 Km
QUATERNARY - CONTINENTAL SEQUENCES
TERTIARY PRECORDILLERA - CONTINENTAL SEQUENCES
TERTIARY FRONTAL CORDILLERA - VOLCANIC SEQUENCES
CRETACEOUS - VOLCANICS SEQUENCES
PALEOZOIC & MESOZOIC BASEMENT
Thrust fault
Inferred Thrust fault
Anticline
Syncline
Lineament
International border
18 ± 0.5Ma.
Radiometric dating

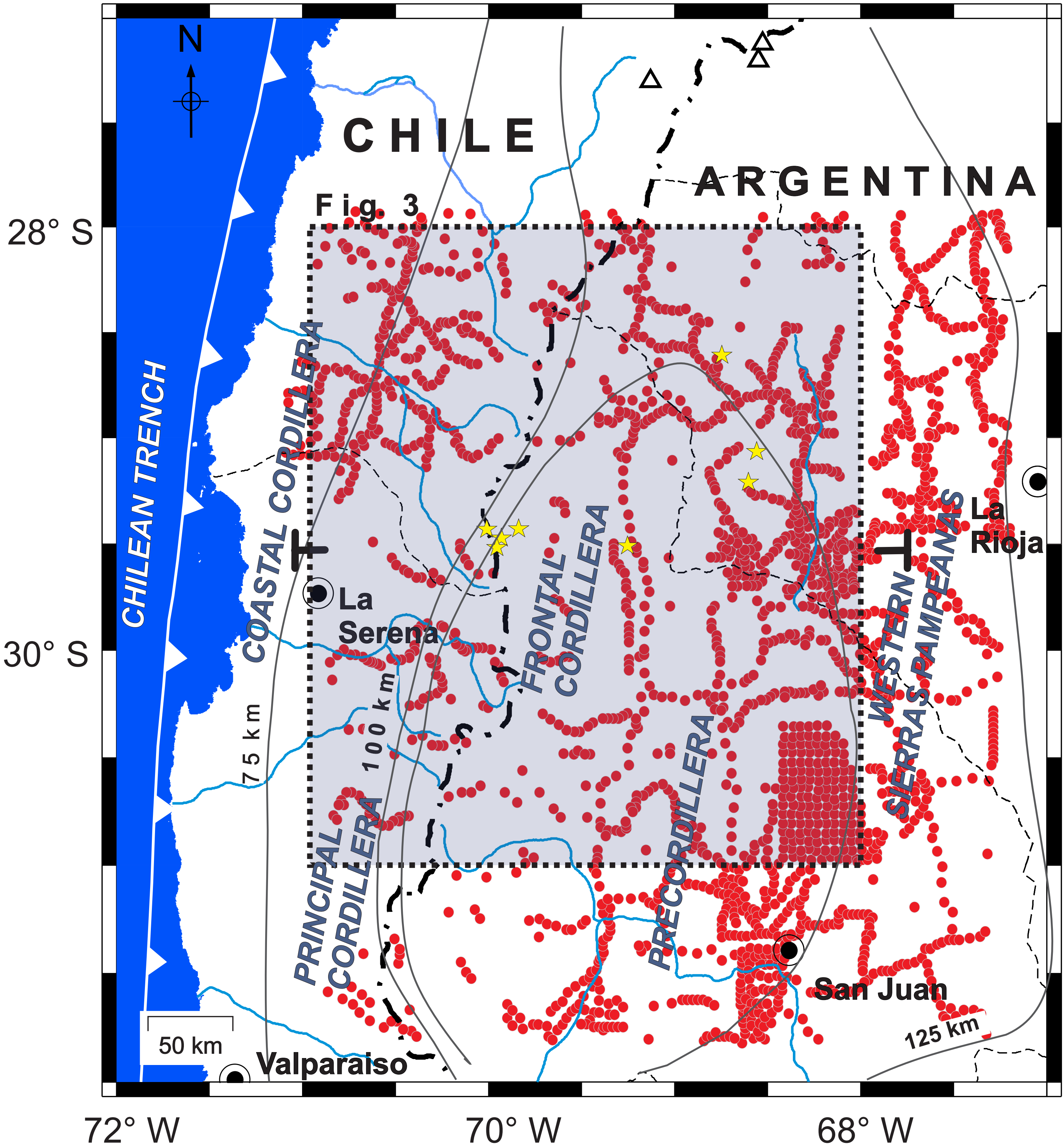

N
CHILE
ARGENTINA
Fig. 3
28° S
30° S
72° W
70° W
68° W
CHILEAN TRENCH
COASTAL CORDILLERA
FRONTAL CORDILLERA
PRINCIPAL CORDILLERA
PRECORDILLERA
WESTERN SIERRAS PAMPEANAS
La Serena
La Rioja
San Juan
Valparaiso
50 km
75 km
100 km
125 km

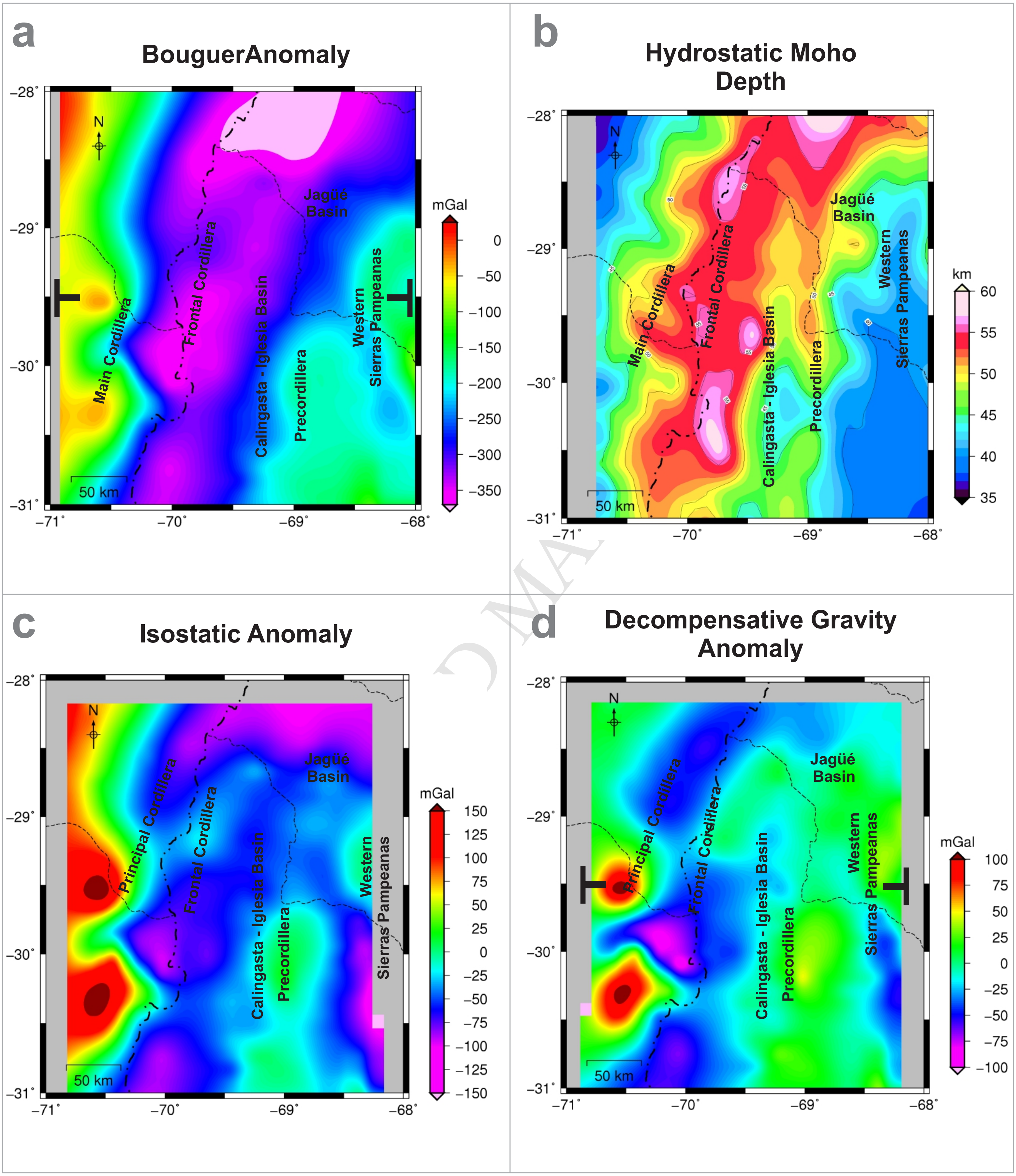
a
BouguerAnomaly
b
Hydrostatic Moho Depth
c
Isostatic Anomaly
d
Decompensative Gravity Anomaly
Main Cordillera
Principal Cordillera
Frontal Cordillera
Calingasta - Iglesia Basin
Precordillera
Jagüé Basin
Western Sierras Pampeanas
50 km
mGal
km
N

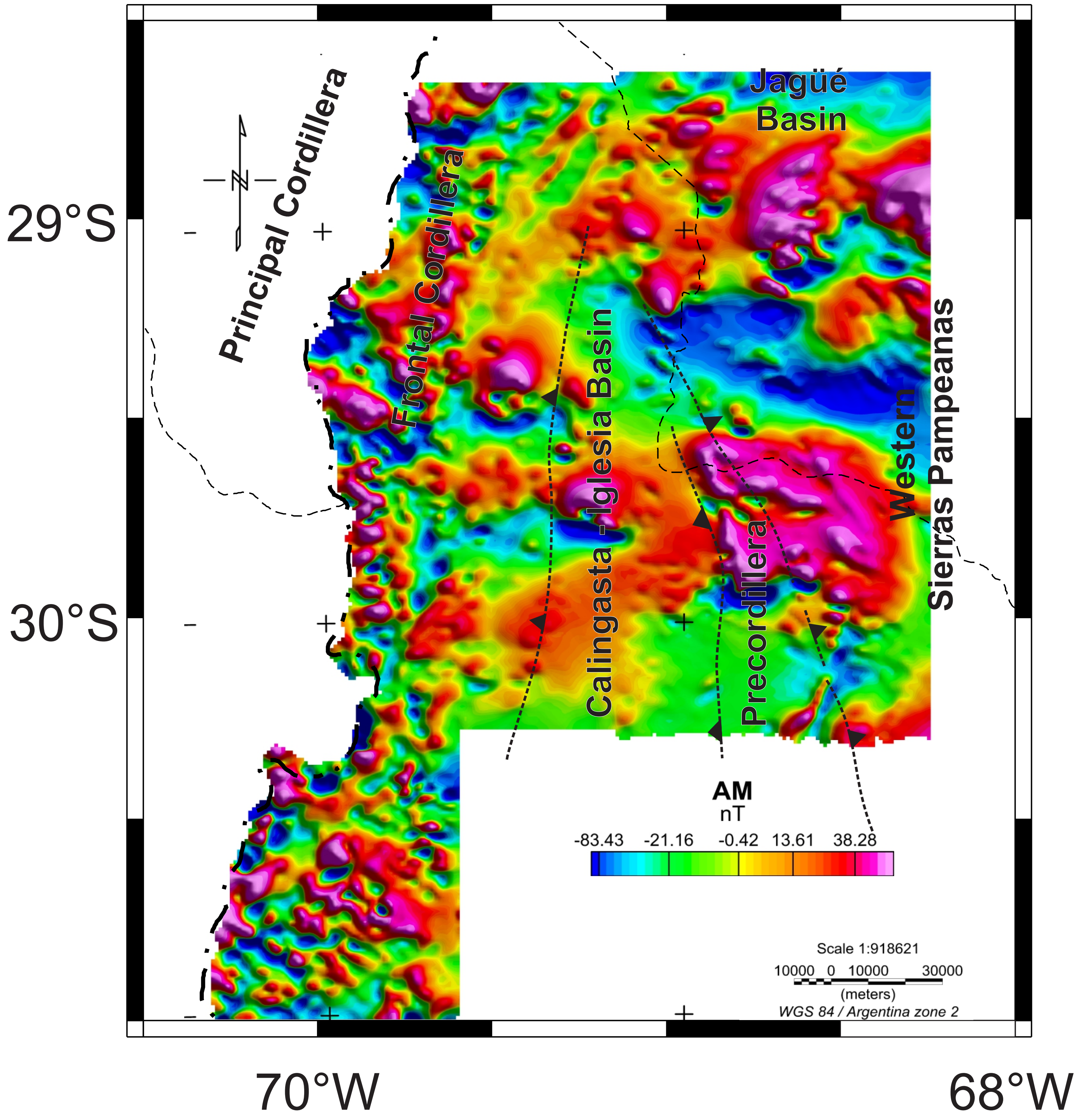
Principal Cordillera
Frontal Cordillera
Jagüé Basin
Calingasta - Iglesia Basin
Precordillera
Western Sierras Pampeanas
29°S
30°S
70°W
68°W
AM
nT
-83.43 -21.16 -0.42 13.61 38.28
Scale 1:918621
10000 0 10000 30000
(meters)
WGS 84 / Argentina zone 2

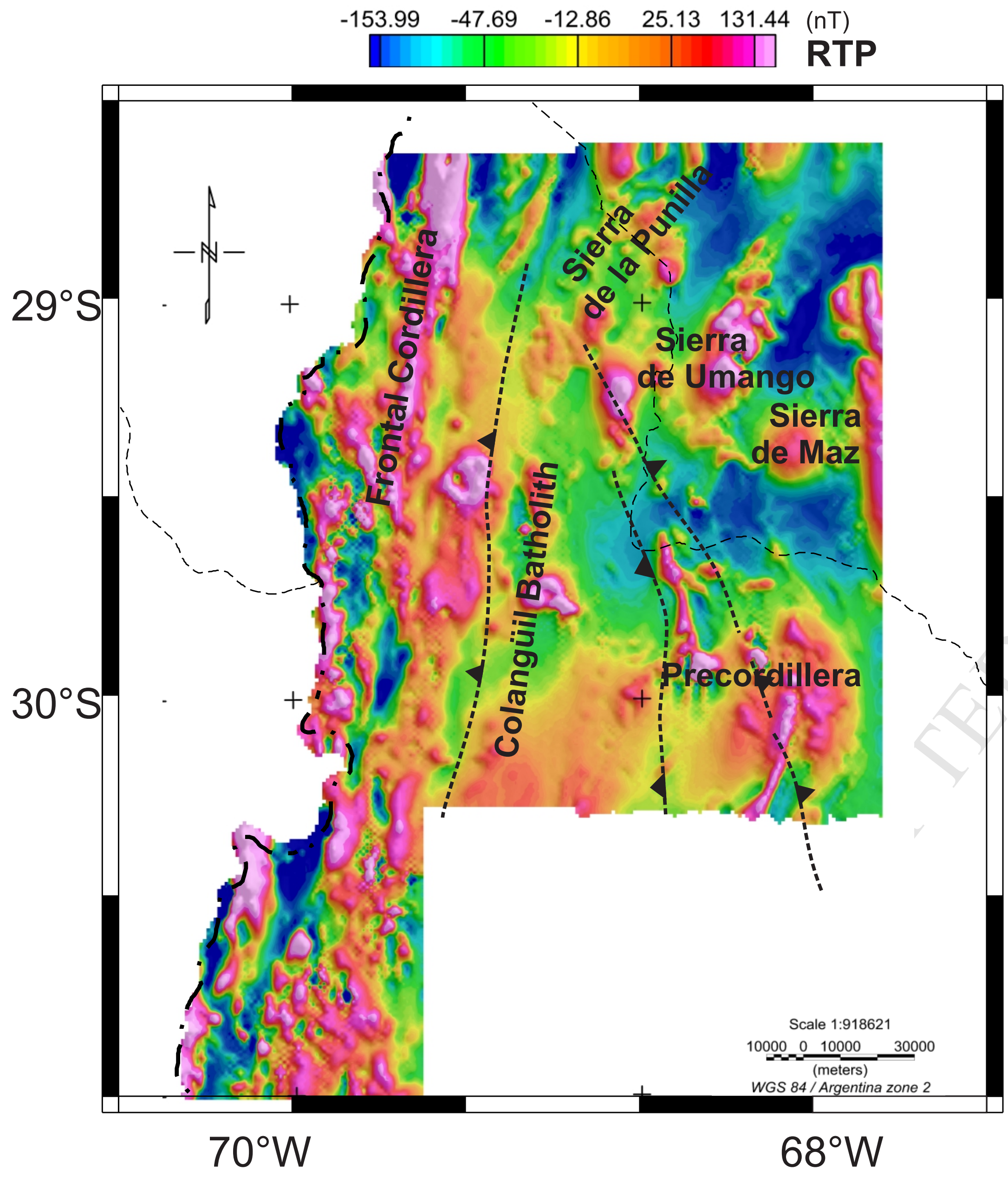

-153.99 -47.69 -12.86 25.13 131.44 (nT)
RTP
29°S
30°S
70°W
68°W
Frontal Cordillera
Sierra de la Punilla
Sierra de Umango
Sierra de Maz
Colangüil Batholith
Precordillera
Scale 1:918621
10000 0 10000 30000
(meters)
WGS 84 / Argentina zone 2

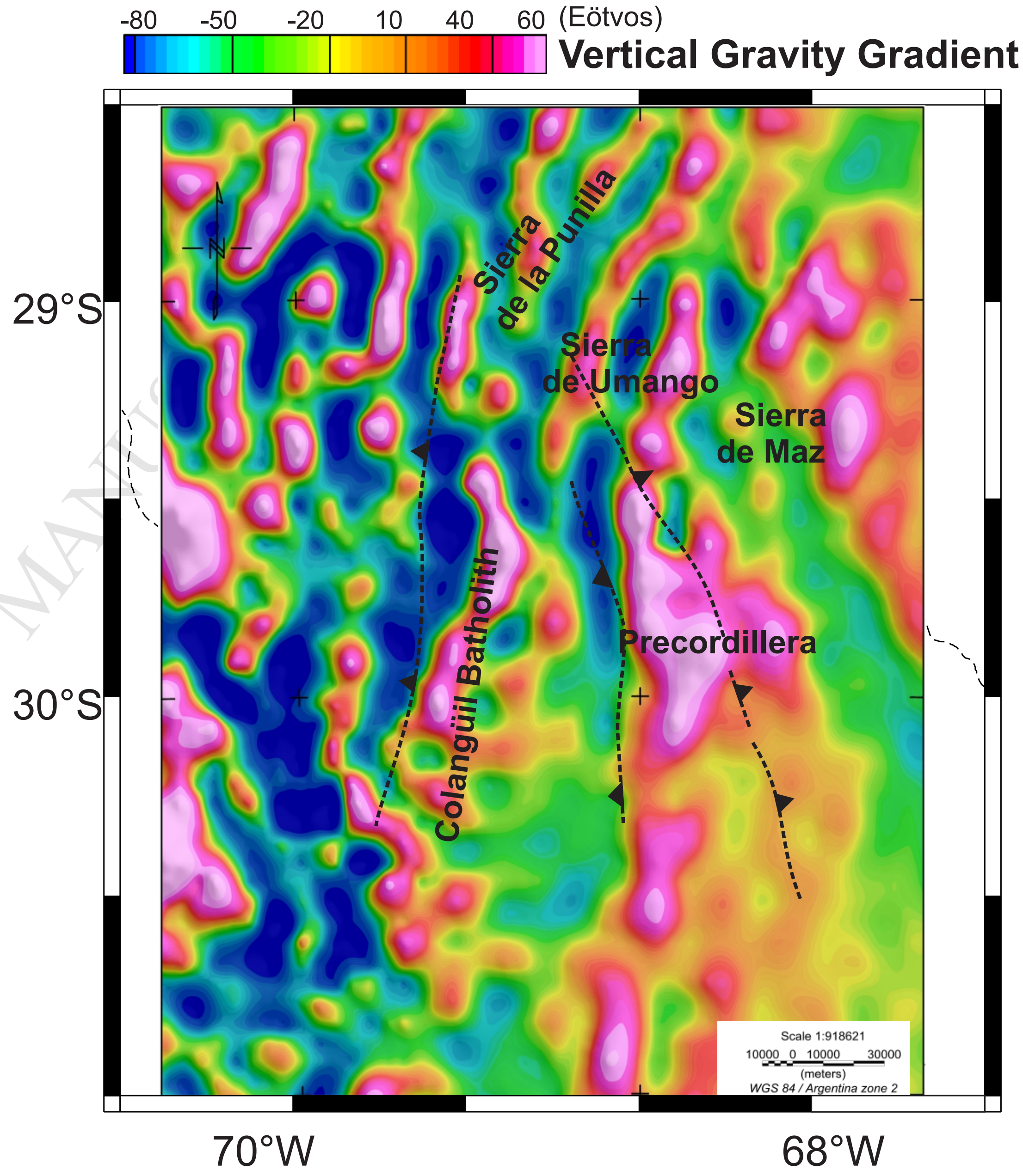

-80 -50 -20 10 40 60 (Eötvos)
Vertical Gravity Gradient
29°S
30°S
70°W
68°W
Sierra de la Punilla
Sierra de Umango
Sierra de Maz
Colangüil Batholith
Precordillera
Scale 1:918621
10000 0 10000 30000
(meters)
WGS 84 / Argentina zone 2

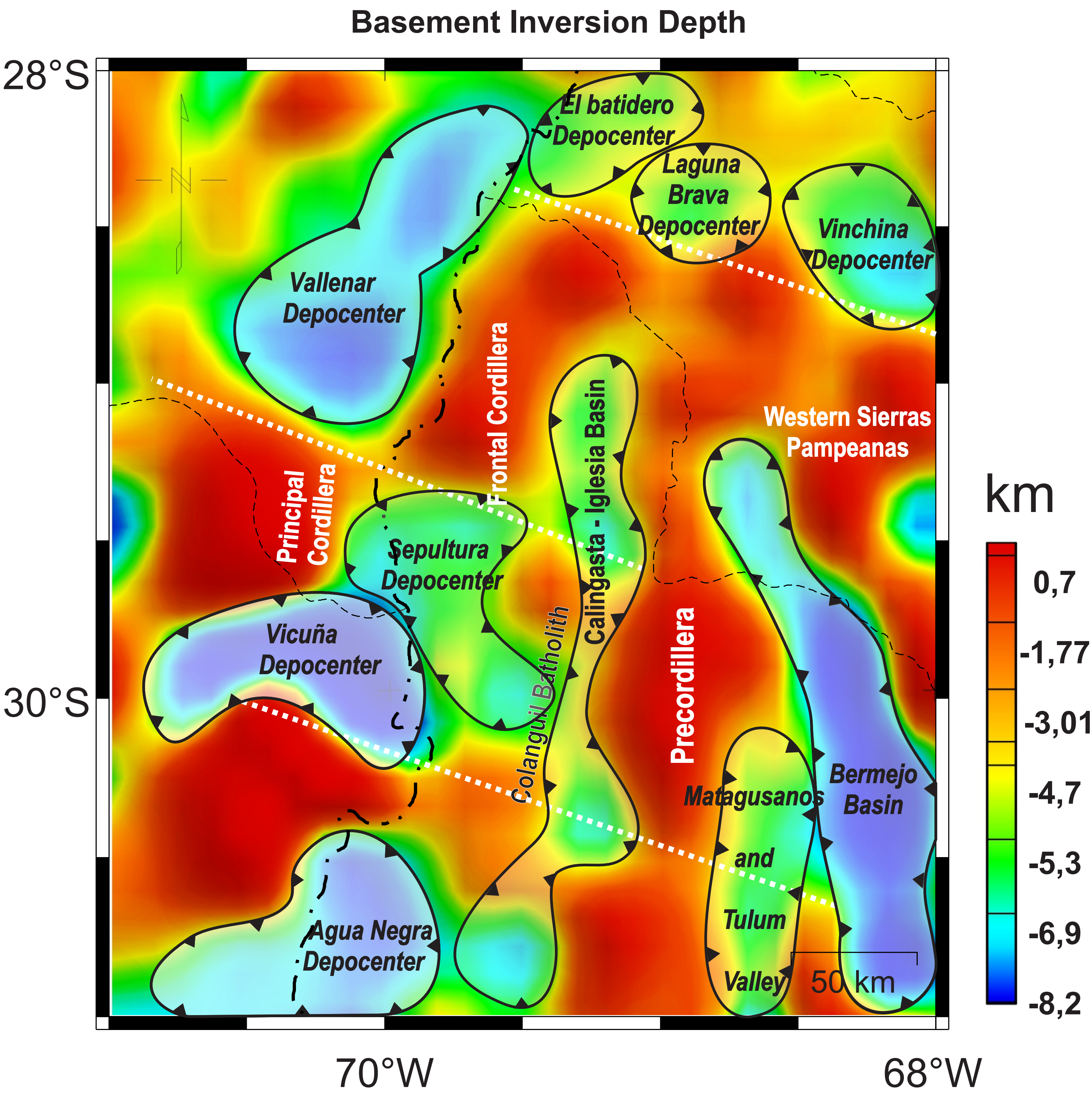
Basement Inversion Depth
28°S
30°S
70°W
68°W
El batidero
Depocenter
Laguna
Brava
Depocenter
Vinchina
Depocenter
Vallenar
Depocenter
Frontal Cordillera
Calingasta - Iglesia Basin
Western Sierras
Pampeanas
Principal
Cordillera
Sepultura
Depocenter
Vicuña
Depocenter
Colanguil Batholith
Precordillera
Matagusanos
and
Tulum
Valley
Bermejo
Basin
Agua Negra
Depocenter
50 km
km
0,7
-1,77
-3,01
-4,7
-5,3
-6,9
-8,2

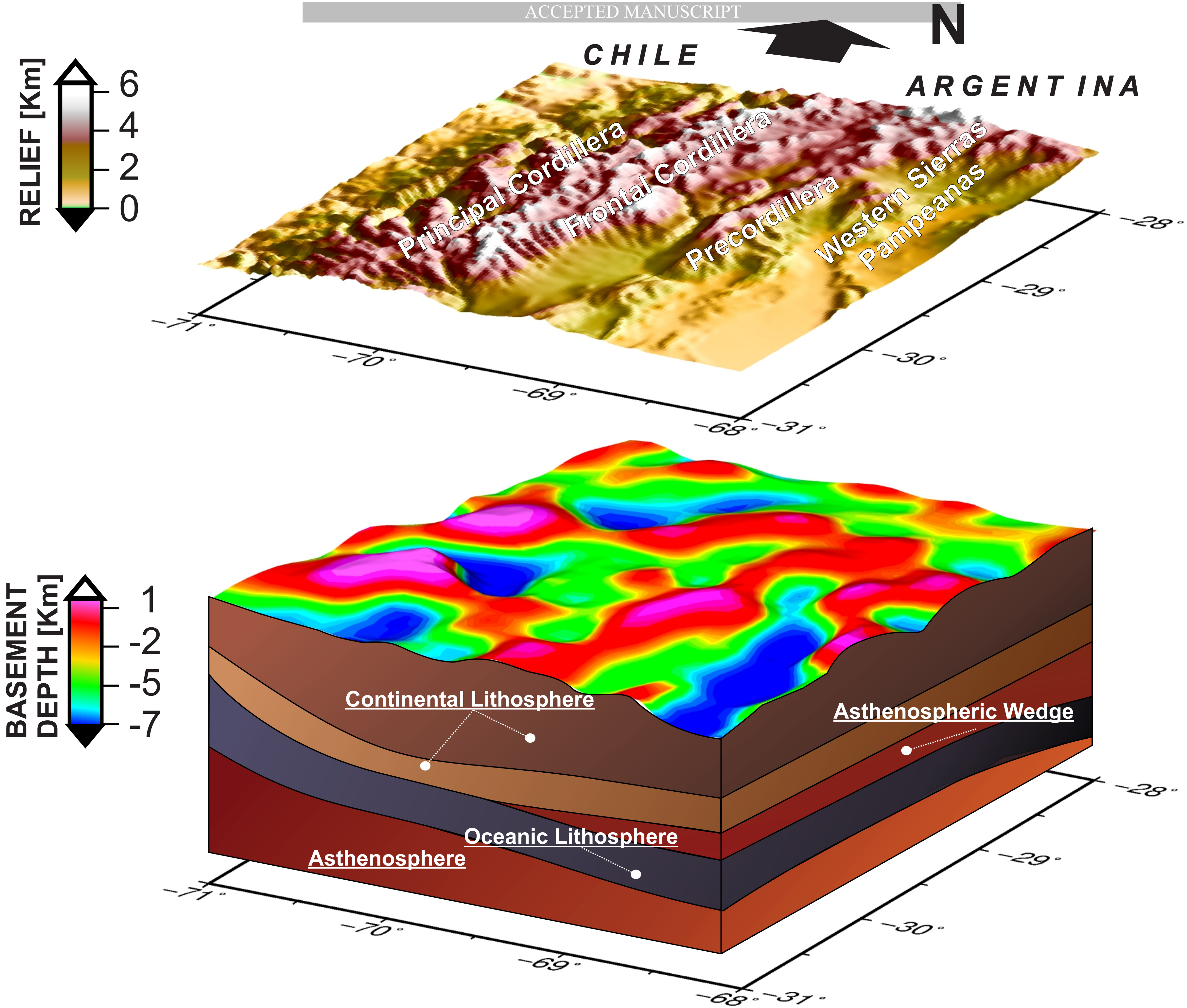

N
CHILE
ARGENTINA
RELIEF [Km]
6
4
2
0
Principal Cordillera
Frontal Cordillera
Precordillera
Western Sierras Pampeanas
-71°
-70°
-69°
-68°
-28°
-29°
-30°
-31°
BASEMENT DEPTH [Km]
1
-2
-5
-7
Continental Lithosphere
Asthenospheric Wedge
Oceanic Lithosphere
Asthenosphere
-71°
-70°
-69°
-68°
-28°
-29°
-30°
-31°

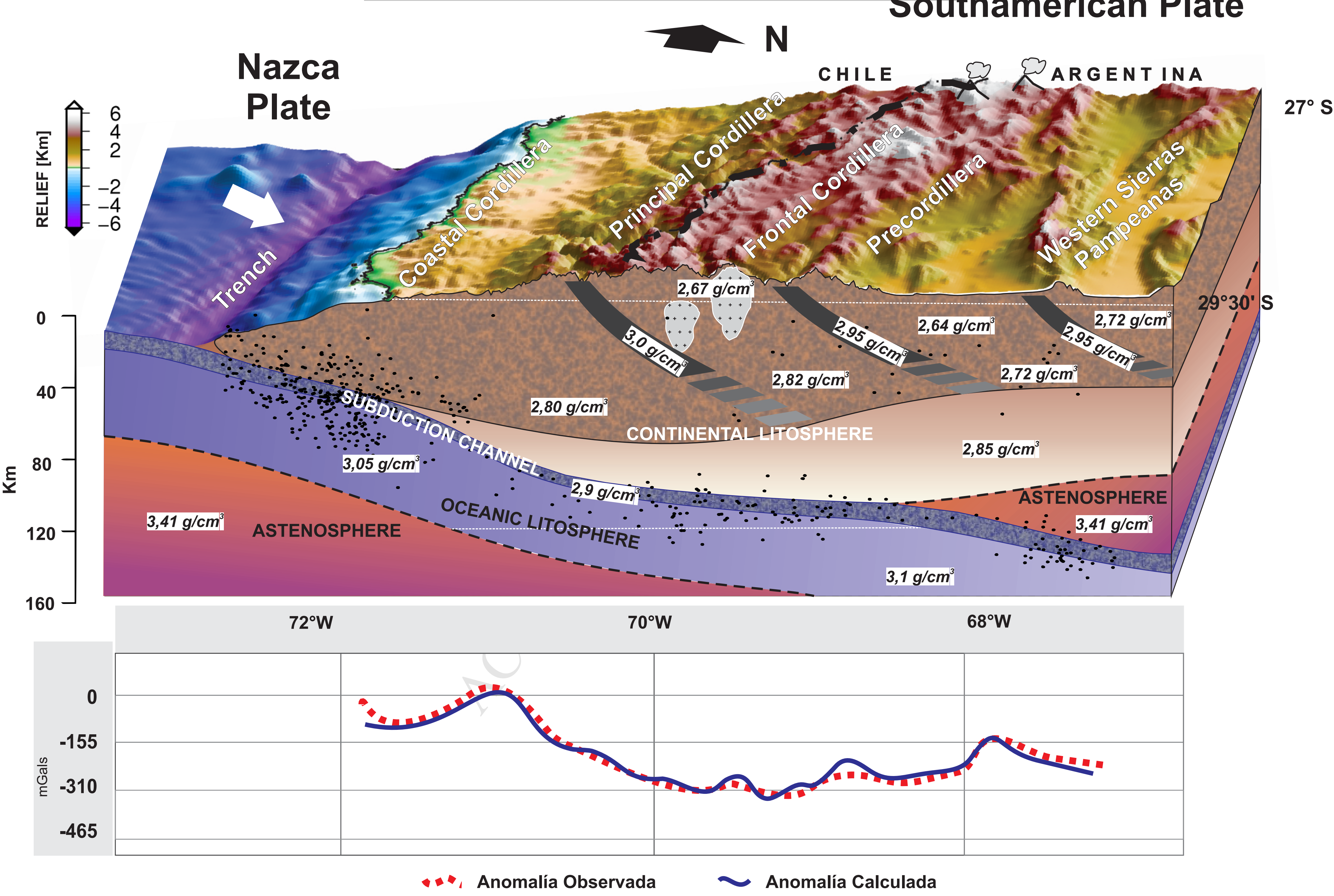
Southamerican Plate
N
Nazca Plate
CHILE
ARGENTINA
27° S
RELIEF [Km]
6
4
2
−2
−4
−6
Trench
Coastal Cordillera
Principal Cordillera
Frontal Cordillera
Precordillera
Western Sierras Pampeanas
29°30' S
0
40
80
120
160
Km
2,67 g/cm³
3,0 g/cm³
2,95 g/cm³
2,64 g/cm³
2,72 g/cm³
2,95 g/cm³
2,82 g/cm³
2,72 g/cm³
2,80 g/cm³
SUBDUCTION CHANNEL
CONTINENTAL LITOSPHERE
2,85 g/cm³
3,05 g/cm³
2,9 g/cm³
ASTENOSPHERE
3,41 g/cm³
ASTENOSPHERE
OCEANIC LITOSPHERE
3,41 g/cm³
3,1 g/cm³
72°W
70°W
68°W
0
-155
-310
-465
mGals
Anomalía Observada
Anomalía Calculada

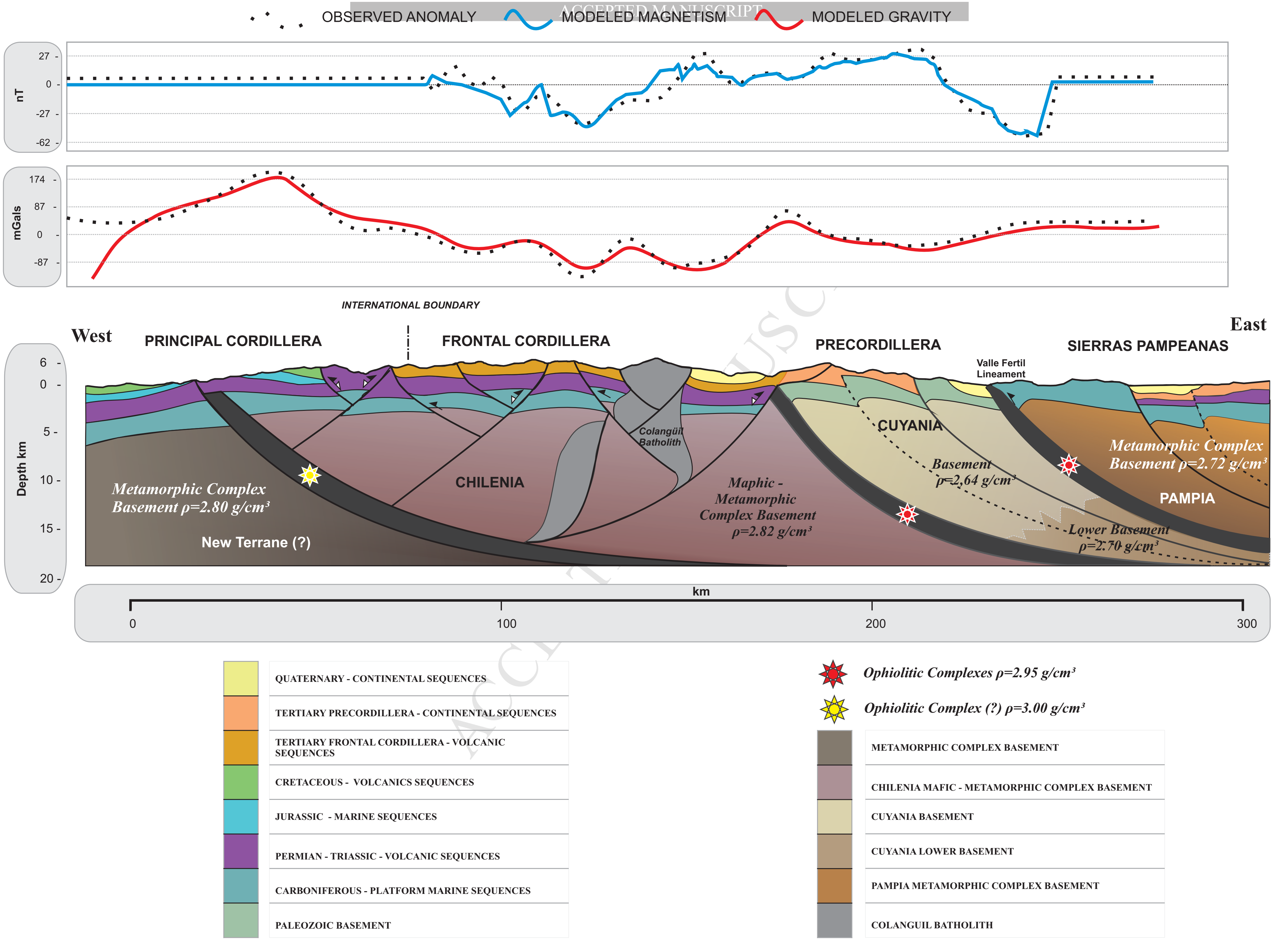
OBSERVED ANOMALY
MODELED MAGNETISM
MODELED GRAVITY
nT
27
0
-27
-62
mGals
174
87
0
-87
INTERNATIONAL BOUNDARY
West
East
PRINCIPAL CORDILLERA
FRONTAL CORDILLERA
PRECORDILLERA
SIERRAS PAMPEANAS
Valle Fertil Lineament
Depth km
6
0
5
10
15
20
Colangüil Batholith
CHILENIA
CUYANIA
PAMPIA
Metamorphic Complex Basement ρ=2.80 g/cm³
New Terrane (?)
Maphic - Metamorphic Complex Basement ρ=2.82 g/cm³
Basement ρ=2.64 g/cm³
Lower Basement ρ=2.70 g/cm³
Metamorphic Complex Basement ρ=2.72 g/cm³
km
0
100
200
300
QUATERNARY - CONTINENTAL SEQUENCES
TERTIARY PRECORDILLERA - CONTINENTAL SEQUENCES
TERTIARY FRONTAL CORDILLERA - VOLCANIC SEQUENCES
CRETACEOUS - VOLCANICS SEQUENCES
JURASSIC - MARINE SEQUENCES
PERMIAN - TRIASSIC - VOLCANIC SEQUENCES
CARBONIFEROUS - PLATFORM MARINE SEQUENCES
PALEOZOIC BASEMENT
Ophiolitic Complexes ρ=2.95 g/cm³
Ophiolitic Complex (?) ρ=3.00 g/cm³
METAMORPHIC COMPLEX BASEMENT
CHILENIA MAFIC - METAMORPHIC COMPLEX BASEMENT
CUYANIA BASEMENT
CUYANIA LOWER BASEMENT
PAMPIA METAMORPHIC COMPLEX BASEMENT
COLANGUIL BATHOLITH

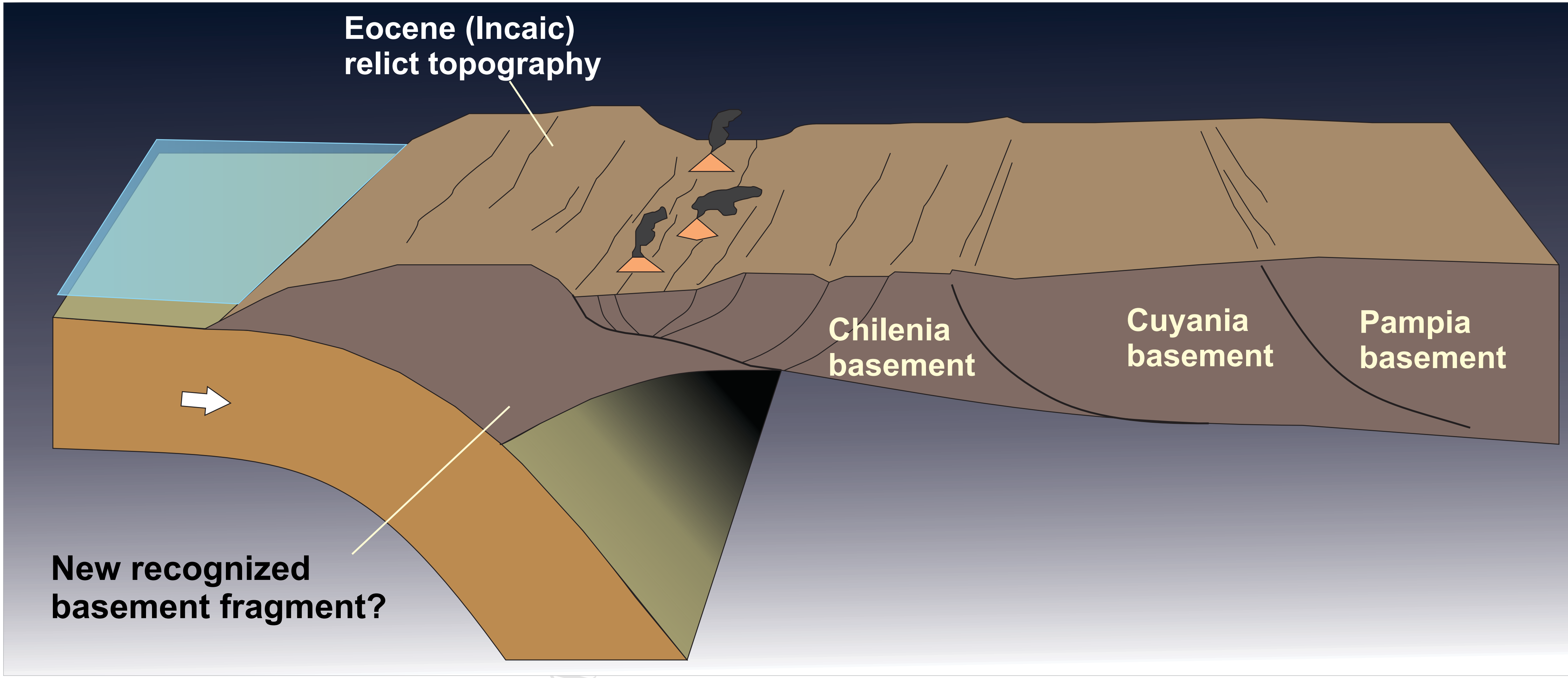
Eocene (Incaic)
relict topography
Chilenia
basement
Cuyania
basement
Pampia
basement
New recognized
basement fragment?

Highlights

- Gravity inversion to obtain the geometry of the Doña Ana abanico basin.
- Determination of main Depocenters from the Andes Range to Western Sierras Pampeanas.
- Remanent Magnetism determination by the Poisson's Theorem.
- Crustal Structure of the late Oligocene Miocene sequences located on Principal Andes.